



1 **Assessing Climate Change-Induced Flood Risk in the**
2 **Conasauga River Watershed: An Application of Ensemble**
3 **Hydrodynamic Inundation Modeling**

4
5 Tigstu T. Dullo,¹ Sudershan Gangrade,^{2,3} Mario Morales-Hernández,^{3,4} Md Bulbul
6 Sharif,⁵ Alfred J. Kalyanapu,^{1,*} Shih-Chieh Kao,^{2,3} Sheikh Ghafoor,⁵ and Moetasim
7 Ashfaq^{3,4}

8
9
10 ¹ Department of Civil and Environmental Engineering, Tennessee Technological
11 University, Cookeville, TN 38505, USA

12 ² Environmental Sciences Division, Oak Ridge National Laboratory, Oak Ridge, TN
13 37831, USA

14 ³ Climate Change Science Institute, Oak Ridge National Laboratory, Oak Ridge, TN
15 37831, USA

16 ⁴ Computational Sciences and Engineering Division, Oak Ridge National Laboratory,
17 Oak Ridge, TN 37831, USA

18 ⁵ Department of Computer Science, Tennessee Technological University, Cookeville, TN
19 38505, USA

20

21

22

23

24

25

26

27

28

29

30 *Corresponding Author

31 Alfred J. Kalyanapu, PhD

32 1020 Stadium Drive, P O Box 5015

33 Cookeville, TN 38505

34 Telephone: 931-372-3561

35 Email Address: akalyanapu@tntech.edu

36

37

38 Notice: This manuscript has been authored by UT-Battelle, LLC, under contract DE-AC05-
39 00OR22725 with the US Department of Energy (DOE). The US government retains and the
40 publisher, by accepting the article for publication, acknowledges that the US government retains a
41 nonexclusive, paid-up, irrevocable, worldwide license to publish or reproduce the published form
42 of this manuscript, or allow others to do so, for US government purposes. DOE will provide
43 public access to these results of federally sponsored research in accordance with the DOE Public
44 Access Plan (<http://energy.gov/downloads/doe-public-access-plan>).

45



46 **Abstract**

47 This study evaluates the impact of potential future climate change on flood regimes,
48 floodplain protection, and electricity infrastructures across the Conasauga River
49 Watershed in the southeastern United States through ensemble hydrodynamic inundation
50 modeling. The ensemble streamflow scenarios were simulated by the Distributed
51 Hydrology Soil Vegetation Model (DHSVM) driven by (1) 1981–2012 Daymet
52 meteorological observations, and (2) eleven sets of downscaled global climate models
53 (GCMs) during the 1966–2005 historical and 2011–2050 future periods. Surface
54 inundation was simulated using a GPU-accelerated Two-dimensional Runoff Inundation
55 Toolkit for Operational Needs (TRITON) hydrodynamic model. Nine out of the eleven
56 GCMs exhibit an increase in the mean ensemble flood inundation areas. Moreover, at the
57 1% annual exceedance probability level, the flood inundation frequency curves indicate a
58 ~16 km² increase in floodplain area. The assessment also shows that even after flood-
59 proofing, four of the substations could still be affected in the projected future period. The
60 increase in floodplain area and substation vulnerability highlights the need to account for
61 climate change in floodplain management. Overall, this study provides a proof-of-
62 concept demonstration of how the computationally intensive hydrodynamic inundation
63 modeling can be used to enhance flood frequency maps and vulnerability assessment
64 under the changing climatic conditions.

65

66 **Keywords:** Flood simulation; Climate change; Critical electricity infrastructure;
67 Floodplain protection standards.



68 **1. Introduction**

69 Floods are costly disasters that affect more people than any other natural hazard
70 around the world (UNISDR, 2015). Major factors that can exacerbate flood damage
71 include population growth, urbanization, and climate change (Birhanu et al., 2016;
72 Winsemius et al., 2016; Alfieri et al., 2017; Alfieri et al., 2018; Kefi et al., 2018). Recent
73 observations exhibit an increase in the frequency and the intensity of extreme
74 precipitation events (Pachauri and Meyer, 2014), which have strengthened the magnitude
75 and frequency of flooding (Milly et al., 2002; Langerwisch et al., 2013; Alfieri et al.,
76 2015a; Alfieri et al., 2018; Mora et al., 2018). As a result, the damage and cost of
77 flooding have substantially increased across the United States (US) (Pielke Jr. and
78 Downton, 2000; Pielke Jr. et al., 2002; Ntelekos et al., 2010; Wing et al., 2018) and the
79 rest of the world (Hirabayashi et al., 2013; Arnell and Gosling, 2014; Alfieri et al.,
80 2015b; Alfieri et al., 2017; Kefi et al., 2018).

81 Since 1968, the National Flood Insurance Program (NFIP), administered by the
82 Federal Emergency Management Agency (FEMA), has implemented floodplain
83 regulation standards in the US to mitigate the escalating flood losses (FEMA, 2002). For
84 communities participating in the NFIP, flood insurance is required for structures located
85 within the 1% annual exceedance probability (AEP) flood zone (i.e., areas with
86 probability of flooding $\geq 1\%$ in any given year; FEMA, 2002). However, existing
87 floodplain protection standards have proven to be inadequate (Galloway et al., 2006;
88 Ntelekos et al., 2010; Tan, 2013; Blessing et al., 2017; HCFCFCD, 2018), and climate
89 change can likely exacerbate these issues (Olsen, 2006; Ntelekos et al., 2010; Kollat et
90 al., 2012; AECOM, 2013; Wobus et al., 2017; Nyaupane et al., 2018; Pralle, 2019). For



91 instance, the streamflow AEP thresholds and synthetic hydrographs used to simulate the
92 flood zones were derived purely based on historic observations that may underestimate
93 the intensified hydrologic extremes in the projected future climatic conditions. Although
94 the possible change of future streamflow AEP thresholds may be evaluated by an
95 ensemble of hydrologic model outputs driven by multiple downscaled and bias-corrected
96 climate models (e.g., Wobus et al., 2017), the extension from maximum streamflow to
97 maximum flood zone is not trivial, and cannot be explicitly addressed through the
98 conventional deterministic inundation modeling approach.

99 The increases in the magnitude and frequency of flooding, in addition to the
100 inadequacy of floodplain measures and the high costs of hardening (Wilbanks et al.,
101 2008; Farber-DeAnda et al., 2010; Gilstrap et al., 2015), have put electricity
102 infrastructures at risk (Zamuda et al., 2015; Zamuda and Lippert, 2016; Cronin et al.,
103 2018; Forzieri et al., 2018; Mikellidou et al., 2018; Allen-Dumas et al., 2019). In
104 particular, electricity infrastructures which lie in areas vulnerable to flooding can
105 experience floodwater damages that may lead to changes in their energy production and
106 consumption (Chandramowli and Felder, 2014; Ciscar and Dowling, 2014; Bollinger and
107 Dijkema, 2016; Gangrade et al., 2019). For instance, flooding can rust metals, destroy
108 insulation, and damage interruption capacity (Farber-DeAnda et al., 2010; Vale, 2014;
109 NERC, 2018; Bragatto et al., 2019). It is estimated that nearly 300 energy facilities are
110 located on low-lying lands vulnerable to sea-level rise and flooding in the lower 48 US
111 states, (Strauss and Ziemplinski, 2012).

112 Several studies have assessed the vulnerability of electricity infrastructures to
113 flooding (Reed et al., 2009; Winkler et al., 2010; Bollinger and Dijkema, 2016; Fu et al.,



114 2017; Pant et al., 2017; Bragatto et al., 2019; Gangrade et al., 2019). Although some of
115 these studies focused on evaluating the resilience of electricity infrastructures against
116 flood hazard and/or climate change, only a few of them evaluated site-specific inundation
117 risk and quantified impacts of climate change-induced flooding on electricity
118 infrastructures under different future climate scenarios. Again, one main challenge is
119 associated with the high computational costs to effectively transform ensemble
120 streamflow projections into ensemble surface inundation projections through
121 hydrodynamic models. With the enhanced inundation models and high performance
122 computing (HPC) capabilities (Morales-Hernández et al., 2020a), this challenge can be
123 gradually overcome for more spatially explicit flood vulnerability assessment.

124 The objective of this study is to demonstrate the applicability of a computationally
125 intensive ensemble inundation modeling approach to better understand how climate
126 change may affect flood regimes, floodplain regulation standards, and the vulnerability of
127 existing infrastructures. The unique aspects of this study are the application of an
128 integrated climate-hydrologic-hydraulic modeling framework for:

- 129 (1) Evaluating the changes in flood regime using high-resolution ensemble flood
130 inundation maps. The ensemble-based approach is able to incorporate the large
131 hydrologic interannual variability and model uncertainty that cannot be captured
132 through the conventional deterministic flood map.
- 133 (2) Enabling direct frequency analysis of ensemble flood inundation maps that
134 correspond to historic and projected future climate conditions. This approach
135 provides an alternative floodplain delineation technique to the conventional



136 approach, in which a single deterministic design flood value is used to develop a
137 flood map with a given exceedance probability.

138 (3) Evaluating the vulnerability of electricity infrastructures to climate change-
139 induced flooding and assessing the adequacy of existing flood protection
140 measures using ensemble flood inundation. This information will help floodplain
141 managers to identify the most vulnerable infrastructures and recommend suitable
142 adaptation measures.

143 The following technique was adopted in this study. First, we generated streamflow
144 projection by utilizing an ensemble of simulated streamflow hydrographs driven by both
145 historical observations and downscaled climate projections (Gangrade et al., 2020) as
146 inputs for hydrodynamic inundation modeling as presented in section 2.2. Then, we set
147 up and calibrated a 2D hydrodynamic inundation model, Two-dimensional Runoff
148 Inundation Toolkit for Operational Needs (TRITON; Morales-Hernández et al., 2020b),
149 in our study area which is presented in section 2.3. For inundation modeling, sensitivity
150 analyses were conducted on three selected parameters to quantify and compare their
151 respective influences on modeled flood depths and extents. The performance of TRITON
152 was then evaluated by comparing a simulated 1% AEP flood map with the reference 1%
153 AEP flood map from the Federal Emergency Management Agency (FEMA). Finally, as
154 presented in sections 2.4 and 2.5, ensemble inundation modeling was performed to
155 develop flood inundation frequency curves and maps, and to assess the vulnerability of
156 electricity infrastructures under a changing climate, respectively.

157 The article is organized as follows: the data and methods are discussed in Section 2;
158 Section 3 presents the result and discussion; and the summary is presented in Section 4.

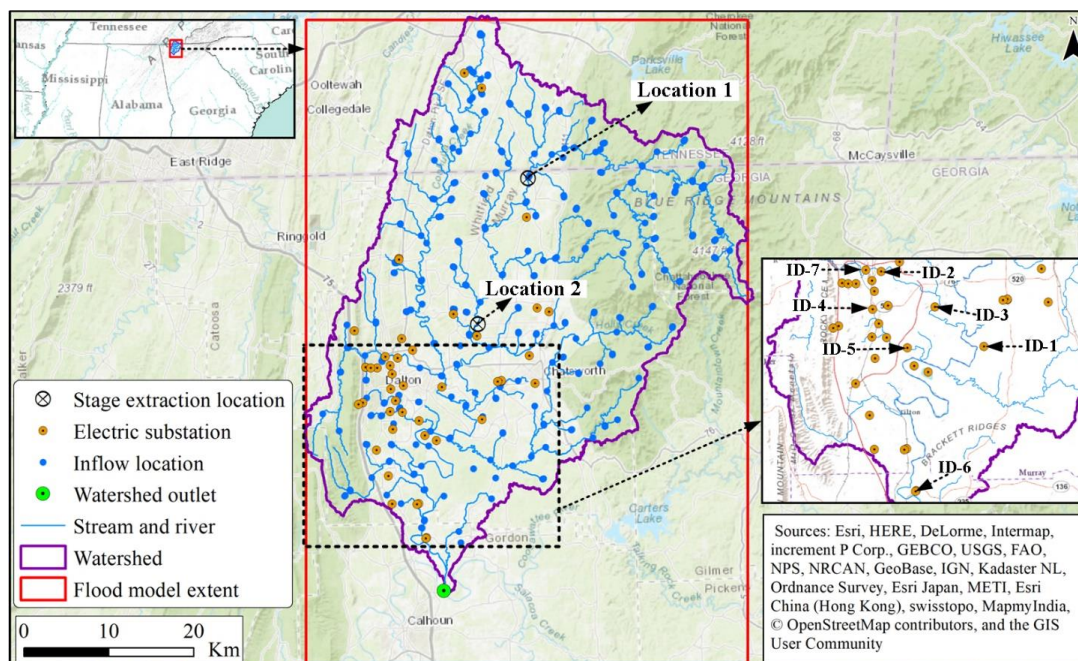


159 **2. Data and Methods**

160 **2.1. Study Area**

161 Our study area is the Conasauga River Watershed (CRW) located in southeastern
162 Tennessee and northwestern Georgia (Figure 1). The CRW is an eight-digit Hydrologic
163 Unit Code (HUC08) subbasin (03150101) with a total drainage area of ~1880 km². The
164 northeastern portions of the watershed are rugged, mountainous areas largely covered
165 with forests (Ivey and Evans, 2000; Elliott and Vose, 2005). The CRW, which is one
166 headwater basin of the Alabama-Coosa-Tallapoosa (ACT) River Basin, rises high on the
167 Blue Ridge Mountains of Georgia and Tennessee and flows for 145 km before joining the
168 Coosawattee River to form the Oostanaula River (Ivey and Evans, 2000; USACE, 2013).
169 The CRW climate is characterized by warm, humid summers, and mild winters with
170 mean annual temperature of 15 to 20 °C and average annual precipitation of 1300 to 1400
171 mm (FIS, 2007; FIS, 2010; Baechler et al., 2015). The watershed encompasses four
172 counties: Bradley, Polk, Fannin, Murray, and Whitfield. It also includes the cities of
173 Dalton and Chatsworth, Georgia. There is no major reservoir located in the CRW.

174



175

176 Figure 1. Conasauga River Watershed study area location, model extent, electric
177 substations, and inflow locations. Background layer source: © OpenStreetMap
178 contributors 2020. Distributed under a Creative Commons BY-SA License.

179

180 2.2. Streamflow Projections

181 The ensemble streamflow projections were generated by a hierarchical modeling
182 framework, which started with regional climate downscaling followed by hydrologic
183 modeling (Gangrade et al., 2020). The climate projections were generated by dynamically
184 downscaling of 11 GCMs from the Coupled Model Intercomparison Project Phase-5
185 (CMIP5) data archive. Each GCM was used as lateral and lower boundary forcing in a
186 regional climate model RegCM4 (Giorgi et al., 2012) at a horizontal grid spacing of 18
187 km over a domain that covered continental US and parts of Canada and Mexico (Ashfaq
188 et al., 2016) (Table 1). Each RegCM4 integration covered 40 years in the historic period



189 (1966–2005; hereafter baseline) and another 40 years in the future period (2011–2050)
190 under Representative Concentration Pathway 8.5 (RCP 8.5) emission scenario, with a
191 combined 880 years of data across all RegCM4 simulations.

192

193 Table 1. Summary of the 11 dynamically downscaled climate models (adopted from
194 Ashfaq et al., 2016).

S. No.	Climate model name	Number of flood events per climate model	Time period	
1	ACCESS1-0			
2	BCC-CSM1-1			
3	CCSM4			
4	CMCC-CM			
5	FGOALS-g2		1966–2005	2011–2050
6	GFDL-ESM2M	40	(Baseline)	(Future/RCP
7	MIROC5			8.5)
8	MPI-ESM-MR			
9	MRI-CGCM3			
10	NorESM1-M			
11	IPSL-CM5A-LR			

195

196 The RegCM4 simulated daily precipitation and temperature were further statistically
197 bias-corrected to a spatial resolution of 4 km following a quantile mapping technique,
198 described in Ashfaq et al. (2010, 2013). The 4 km Parameter-elevation Regressions on
199 Independent Slopes Model (PRISM; Daly et al., 2008) data was used as the historic
200 observations to support bias-correction. In the baseline period, the simulated quantiles of
201 precipitation and temperature were corrected by mapping them onto the observed



202 quantiles. In the future period, the monthly quantile shifts were calculated based on the
203 simulated baseline and future quantiles which were subsequently added to the bias
204 corrected baseline quantiles to generate bias-corrected monthly future data. Finally, the
205 monthly bias-corrections were distributed to the daily values while preserving in each
206 time period. This approach substantially improves the biases in the modeled daily
207 precipitation and temperature while preserving the simulated climate change signal.
208 Further details of the bias-correction are provided in Ashfaq et al. (2010, 2013) while the
209 information regarding the RegCM4 configuration, evaluation and future climate
210 projections are detailed in Ashfaq et al. (2016).

211 The hydrologic simulations were then conducted using the Distributed Hydrology
212 Soil Vegetation Model (DHSVM; Wigmosta et al., 1994), which is a process-based high-
213 resolution hydrologic model that can capture heterogeneous watershed processes and
214 meteorology at a fine resolution. DHSVM uses spatially distributed parameters, including
215 topography, soil types, soil depths, and vegetation types. The input meteorological data
216 includes precipitation, incoming shortwave and longwave radiation, relative humidity, air
217 temperature and wind speed (Wigmosta et al., 1994; Storck et al., 1998; Wigmosta et al.,
218 2002). The DHSVM performance and applicability has been reported in various earlier
219 climate and flood related studies (Elsner et al., 2010; Hou et al., 2019; Gangrade et al.,
220 2018, 2019, 2020). A calibrated DHSVM implementation from Gangrade et al. (2018) at
221 90 m grid spacing was used to produce 3-hourly streamflow projections using the
222 RegCM4 meteorological forcings described in the previous section (Table 1). In addition,
223 a control simulation driven by 1981–2012 Daymet meteorologic forcings (Thornton et
224 al., 1997) was conducted for model evaluation and validation. The hydrologic simulations



225 used in this study are a part of a larger hydroclimate assessment effort for the ACT River
226 Basin, as detailed in Gangrade et al. (2020). Since there is no major reservoir in the
227 CRW, the additional reservoir operation module (Zhao et al., 2016) was not needed in
228 this study.

229 Note that while the ensemble streamflow projections based on dynamical
230 downscaling and high-resolution hydrologic modeling from Gangrade et al. (2020) are
231 suitable to explore extreme hydrologic events in this study, they do not represent the full
232 range of possible future scenarios. Additional factors such as other GCMs, RCP
233 scenarios, downscaling approaches, and hydrologic models and parameterization may
234 also affect future streamflow projections. In other words, although these ensemble
235 streamflow projections can tell us how likely the future streamflow magnitude may
236 change from the baseline level, they are not the absolute prediction into the future. In
237 practice, these modeling choices will likely be study-specific based on the agreement
238 among key stakeholders. It is also noted that the new Coupled Model Intercomparison
239 Project Phase-6 (CMIP6) data have also become available to update the ensemble
240 streamflow projections, but is not pursued in this study.

241 **2.3. Inundation Modeling**

242 The ensemble inundation modeling was performed using TRITON, which is a
243 computationally enhanced version of Flood2D-GPU (Kalyanapu et al., 2011). TRITON
244 allows parallel computing using multiple graphics processing units (GPUs) through a
245 hybrid Message Passing Interface (MPI) and Compute Unified Device Architecture
246 (CUDA) (Morales-Hernández et al., 2020b). TRITON solves the nonlinear hyperbolic
247 shallow water equations using an explicit upwind finite-volume scheme, based on Roe's



248 linearization. The shallow water equations are a simplified version of the Navier-Stokes
249 equations in which the horizontal momentum and continuity equations are integrated in
250 the vertical direction (see Morales-Hernández et al., (2020b), for further model details).
251 An evaluation of TRITON performance for the CRW is presented and discussed in
252 Section 3.3.

253 TRITON's input data includes digital elevation model (DEM), surface roughness,
254 initial depths, flow hydrographs, and inflow source locations (Kalyanapu et al., 2011;
255 Marshall et al., 2018; Morales-Hernández et al., 2020a; Morales-Hernández et al.,
256 2020b). In this study, the hydraulic and geometric parameters from the flood model
257 evaluation section (Section 3.3) were used in the flood simulation. The topography was
258 represented using the one-third arc-second (~10 m) spatial resolution DEM (Archuleta et
259 al., 2017) from the US Geological Survey (USGS). To improve the quality of the base
260 DEM, as discussed in the flood model evaluation section, the main channel elevation was
261 reduced by 0.15 m. Elevated roads and bridges that obstruct the flow of water were also
262 removed. For surface roughness, we used a single channel Manning's n value of 0.05 and
263 a single floodplain Manning's n value of 0.35. The selection of channel and floodplain
264 Manning's n value was based on the Whitfield County Flood Insurance Study (FIS,
265 2007), which reported a range of Manning's n values estimated from field observations
266 and engineering judgment for about 15 streams inside the CRW (section 3.2).
267 Furthermore, a water depth value of 0.35 m was defined for the main river channel as an
268 initial boundary condition. The zero velocity gradients were used as the downstream
269 boundary condition. Further discussion of model parameter sensitivity and model
270 evaluation are provided in sections 3.2 and 3.3.



271 The simulated DHSVM streamflow was used to prepare inflow hydrographs for
272 ensemble inundation modeling. To provide a large sample size for frequency analysis, we
273 selected all annual maximum peak streamflow events (the maximum corresponded to the
274 outlet of CRW [Figure 1]) from the 1981–2012 control simulation (32 years), the 1966–
275 2005 baseline simulation (440 years; 40 years \times 11 models), and the 2011–2050 future
276 simulation (440 years; 40 years \times 11 models), with a total of 912 events. For each annual
277 maximum event, the 3-hour timestep, 10-day hydrographs (which capture the peak CRW
278 outlet discharge) across all DHSVM river segments were summarized. Following a
279 procedure similar to Gangrade et al. (2019), these streamflow hydrographs were
280 converted to TRITON inputs at 300 inflow locations selected along the NHD+ river
281 network in the CRW (Figure 1). The TRITON model extent, shown in Figure 1, has an
282 approximate area of 3945 km² and includes ~44 million model grid cells (7976 rows \times
283 5474 columns in a uniform structured mesh). The ensemble flood simulations resulted in
284 gridded flood depth and velocity output at 30-minute intervals. The simulations generated
285 an approximately 400 Terabyte data and utilized ~2000 node hours on the Summit
286 supercomputer, managed by the Oak Ridge Leadership Computing Facility at Oak Ridge
287 National Laboratory.

288 **2.4. Flood Inundation Frequency Analysis**

289 Given the nature of GCM experiments, each set of climate projections can be
290 considered as a physics-based realization of historic and future climate under specified
291 emission scenarios. Therefore, an ensemble of multimodel simulations can effectively
292 increase the data lengths and sample sizes that are keys to support frequency analysis,
293 especially for low-AEP events. In this study, we conducted flood frequency analyses



294 separately for the 1966–2005 baseline and 2011–2050 future periods so that the
295 difference between the two periods represent the changes in flood risk due to climate
296 change.

297 To prepare the flood frequency analysis, we first calculated the maximum flood depth
298 at every grid in each simulation. A minimum threshold of 10 cm flood depth was used to
299 judge whether a cell was wet or dry (Gangrade et al., 2019). Further, for a given grid cell,
300 if the total number of non-zero flood depth values (i.e., of the 440 depth values) was less
301 than 30, the grid cell was also considered dry. This threshold was selected based on the
302 minimum sample size requirement for flood depth frequency analysis suggested by Li et
303 al. (2018). Next, we calculated the maximum flooded area (hereafter used alternatively
304 with “floodplain area”) for each simulation. A log-Pearson Type III (LP3) distribution
305 was then used for frequency analysis following the guidelines outlined in Bulletins 17B
306 (USGS, 1982; Burkey, 2009) and 17C (England Jr. et al., 2019). Two types of LP3 fitting
307 were performed. The first type of fitting is event-based that fitted LP3 on the maximum
308 inundation area across all ensemble members. The second type of fitting is grid-based
309 (more computationally intensive) that fitted LP3 on the maximum flood depth at each
310 grid cell across all ensemble members. For both types of fittings, the frequency estimates
311 at 4%, 2%, 1%, and 0.5% AEP (corresponding to 25-, 50-, 100-, and 200-year return
312 levels) were derived for further analysis.

313 It is also noted that in addition to the annual maximum event approach used in this
314 study, one may also use the peak-over-threshold (POT) approach which can select
315 multiple streamflow events in a very wet year. While such an approach can lead to higher
316 extreme streamflow and inundation estimates, the timing of POT samples is fully



317 governed by the occurrences of wet years. In other words, if the trend of extreme
318 streamflow is significant in the future period, the POT samples will likely occur more in
319 the far future period. We hence select the annual maximum event approach that can
320 sample maximum streamflow events more evenly in time, which can better capture the
321 evolution of extreme events with time under the influence of climate change.

322 **2.5. Vulnerability of Electricity Infrastructure**

323 The vulnerability of electricity infrastructures to climate change-induced flooding
324 was evaluated using the ensemble flood inundation results. The 44 electric substations
325 (Figure 1) collected from the publicly available Homeland Infrastructure Foundation-
326 Level Data (HIFLD, 2019) were considered to be the electrical components susceptible to
327 flooding. To evaluate the vulnerability of these substations, we overlapped the maximum
328 flood extent from each ensemble member with all substations to identify the substations
329 that might be inundated under the baseline and future climate conditions. Further, as an
330 additional flood hazard indicator, the duration of inundation was estimated at each of the
331 affected substations using the ensemble flood simulation results.

332 The vulnerability analysis was performed for two different flood mitigation scenarios.
333 In the first scenario, we assumed that no flood protection measures were provided at all
334 substations. Hence, the substations that intersected with the flood footprint were
335 considered to be failed. In the second scenario, it was assumed that flood protection
336 measures were adopted for all substations following the FEMA P-1019 recommendation
337 (FEMA, 2014). According to FEMA P-1019 (FEMA, 2014), for emergency power
338 systems within critical facilities, the highest elevation among (1) the base flood elevation
339 (BFE: 1% FEMA AEP flood elevation) plus 3 feet (~0.91 m), (2) the locally adopted



340 design flood elevation, and (3) the 500-year flood elevation can be used to design flood
341 protection measures. Since the three recommended elevations were not available at all
342 substation locations, we focused only on the BFE plus ~0.91 m option. In addition, since
343 in the CRW the majority of existing flood insurance maps were classified as Zone A—
344 meaning that the special flood hazard areas were determined by approximate methods
345 without BFE values (FEMA, 2002)—we used the maximum flood depth values across all
346 control simulation years as the BFE values in this second mitigation scenario.

347 During the vulnerability analysis, we also assumed that (1) the one-third arc-second
348 spatial resolution DEM might reasonably represent the elevation of substations, (2)
349 existing substations would remain functional and would not be relocated, and (3) no
350 additional hardening measures (i.e., protections such as levees, berms, anchors, and
351 housings) will be adopted in the future period. Also, the cascading failure of a substation
352 due to grid interconnection was not considered in this study.

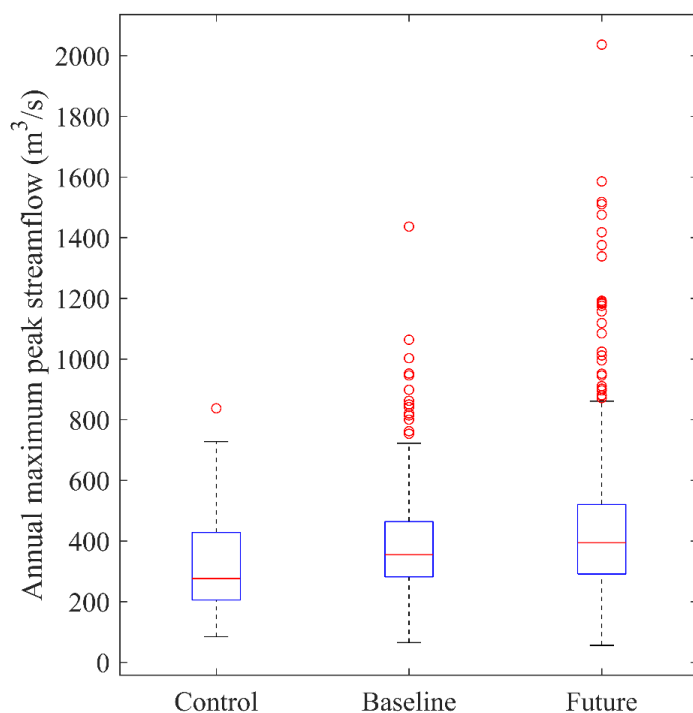
353 **3. Results and Discussion**

354 **3.1. Streamflow Projections**

355 This section presents a comparison of the annual maximum peak streamflow (at the
356 outlet of CRW) used in the control, baseline, and future simulations. The sample size
357 included 32 events from the control (1981–2012) simulation, 440 events from the
358 baseline (1966–2005) simulations, and another 440 events from the future (2011–2050)
359 simulations. These samples are illustrated in box and whisker plots in Figure 2, where
360 central mark indicate the median, while bottom and top edges indicate the 25th and 75th
361 percentiles respectively. The whiskers extend to the furthest data points not considered
362 outliers, which correspond to approximately ± 2.7 standard deviations and 99.3%



363 coverage if the data are normally distributed. As is evident from Figure 2, the
364 distributions of annual maximum peak streamflow values in the control and baseline
365 simulations are comparable. The upper and lower whiskers in the control simulation are
366 $727.6 \text{ m}^3/\text{s}$ and $84.2 \text{ m}^3/\text{s}$, which compare well to the $722.5 \text{ m}^3/\text{s}$ and $65.2 \text{ m}^3/\text{s}$ values in
367 the baseline simulation. A larger number of outliers are present in the baseline
368 simulation, which is due to the larger sample size (440 versus 32). Under the future
369 projection, an increase in the maximum peak streamflow is shown, where the upper
370 whisker in the future projection is ~21% higher than the baseline. Moreover, the
371 maximum of distribution in the future climate ($2036.7 \text{ m}^3/\text{s}$) is also much higher than that
372 in the baseline climate ($1436.7 \text{ m}^3/\text{s}$), suggesting a higher future flood risk in the CRW.
373 The increasing trend of streamflow extremes in the CRW is consistent with the overall
374 findings in the ACT River Basin (Gangrade et al., 2020).



375

376 Figure 2. A comparison of annual maximum peak streamflow at the outlet of Conasauga
377 River Watershed. The sample size includes 32 events from the control (1981–2012), 440
378 from the baseline (1966–2005), and another 440 from the future (2011–2050) periods.

379 3.2. Sensitivity Analysis for Flood Model

380 For a better understanding and selection of suitable TRITON parameters, a series of
381 sensitivity analyses were conducted using different combinations of Manning's
382 roughness, initial water depths, and river bathymetry correction factors (Table 2).

383

384

385



386 Table 2. Summary of hydraulic and geometric parameters used in the sensitivity analysis.

Sensitivity parameter	Scenario	Initial water depth values (m)	Surface roughness (Manning's n values)	Bathymetry correction factor (m)
Initial water depth	1	0.00	$n_{ch} = 0.050 / n_{fldpl} = 0.350$	-0.15
	2	0.15		
	3	0.35		
	4	0.45		
	5	0.55		
	6	0.65		
Surface roughness	1	0.35	$N_1: n_{ch} = 0.035 / n_{fldpl} = 0.06$	-0.15
	2		$N_2: n_{ch} = 0.040 / n_{fldpl} = 0.25$	
	3		$N_3: n_{ch} = 0.045 / n_{fldpl} = 0.30$	
	4		$N_4: n_{ch} = 0.050 / n_{fldpl} = 0.35$	
	5		$N_5: n_{ch} = 0.055 / n_{fldpl} = 0.45$	
	6		$N_6: n_{ch} = 0.060 / n_{fldpl} = 0.50$	
Bathymetry correction factor	1	0.35	$n_{ch} = 0.050 / n_{fldpl} = 0.350$	0.00
	2			-0.15
	3			-0.45
	4			-0.75
	5			-1.00
	6			-1.25

387 Note: n_{ch} represents the Manning's n value in the main channel and n_{fldpl} represents the
 388 Manning's n value in the floodplain areas.

389

390 In calibrating a hydraulic model, it is a common practice to adjust the estimated
 391 Manning's n value, as it is the most uncertain and variable input hydraulic parameter
 392 (Brunner et al., 2016). In this study, we tested six different scenarios (Table 2) based on
 393 the Whitfield County Flood Insurance Study (FIS, 2007), which reported a range of
 394 Manning's n values estimated from field observations and engineering judgment for
 395 about 15 streams inside the CRW. To establish an initial condition for TRITON, a
 396 sensitivity analysis was performed on selected initial water depth values (ranging from
 397 0 m to 0.65 m, Table 2) to understand their relative effects. To select ranges for the initial
 398 water depth, we summarized the observed water depth values that corresponds to low



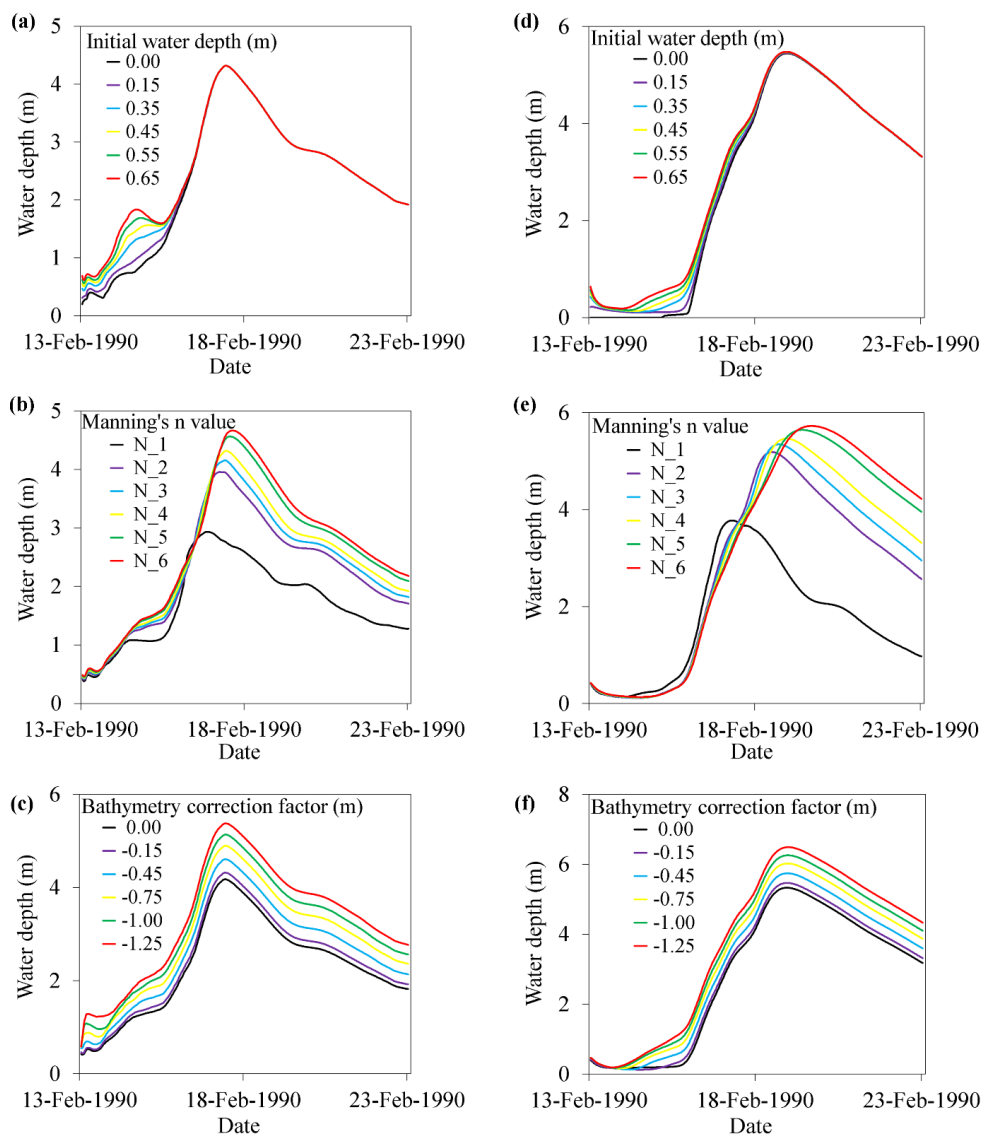
399 flow values at five USGS gauge stations inside the CRW. The distribution of observed
400 water depth values from the five gauges showed average values ranging from 0.25 to
401 0.65m. Existing DEM products, even those with high spatial resolution (i.e., 10 m or
402 finer), do not represent the elevation of river bathymetry accurately (Bhuyian et al.,
403 2014). For the CRW, Bhuyian et al. (2019) found that the one-third arc-second spatial
404 resolution base DEM over-predicted the inundation extent because of the bathymetric
405 error, which reduced the channel conveyance. In this study, we tested various bathymetry
406 correction factors (ranging from -1.25 m to 0 m, Table 2) by reducing the DEM elevation
407 along the main channel to understand the sensitivity of TRITON.

408 The sensitivity analysis was performed using the February 13–22, 1990 flood event
409 that has the maximum discharge among all 32 control simulation events. To evaluate
410 relative sensitivity of TRITON, we extracted simulated flood depths at two arbitrary
411 selected locations (Figure 1) and estimated the relative inundation area differences. The
412 impacts of initial water depths were significant only at the beginning where low flow
413 values dominated the hydrographs (Figure 3a, 3d). Larger initial water depth values
414 generated higher flood inundation depths for both sample locations. Although the
415 differences in flood inundation extents relative to the dry bed show an increasing trend,
416 the relative differences are less than 1.4% (Figure 4a). Increase in the channel and
417 floodplain Manning's n values resulted in higher flood depths for both sample locations
418 (Figure 3b and 3e). The relative flood inundation area differences increase from about
419 23% to 31% (Figure 4b) when the channel and floodplain Manning's n values are
420 increased from 0.035 to 0.06 and from 0.06 to 0.50, respectively. Reduction in the
421 elevation of river bathymetry (to improve the quality of the base DEM) results in a direct



422 increase in maximum flood depth due to change in the river conveyance (Figure 3c and
423 3f). It also results in a decrease in the maximum flood extent (Figure 4c), as more water
424 is allowed to transport through the main channel instead of the floodplain. Overall, the
425 results showed that TRITON was more sensitive to the Manning's n values than the
426 initial water depths and bathymetric correction factors.

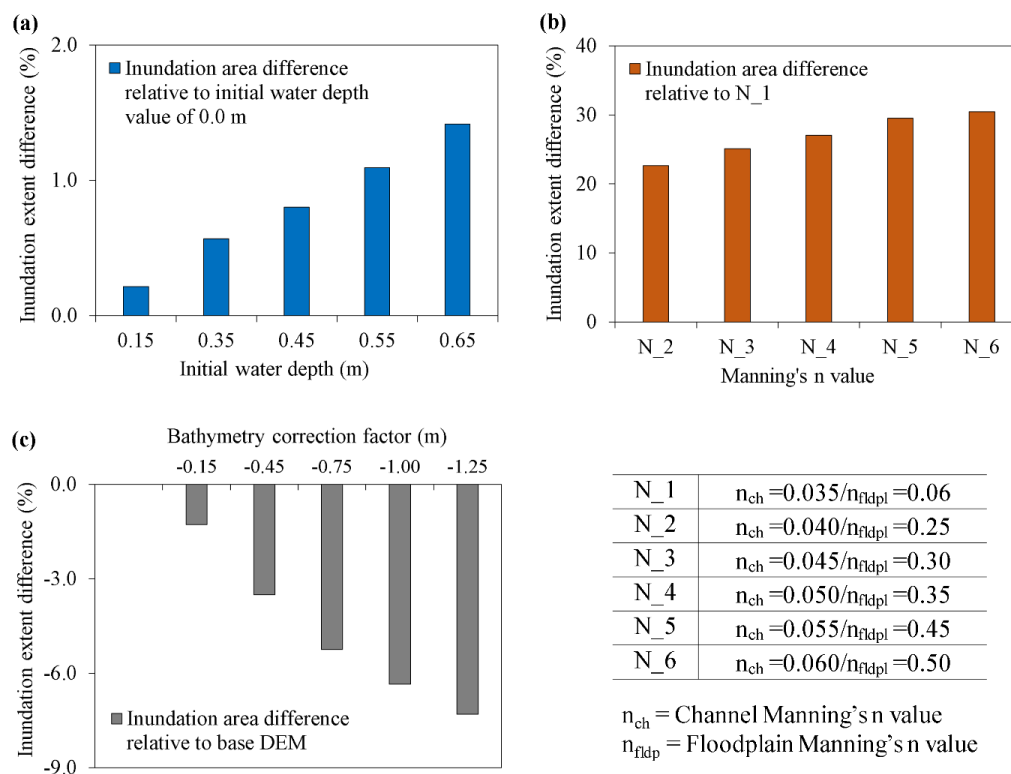
427



428

429 Figure 3. Simulated flood inundation depths extracted at location 1 (a, b, c) and at
430 location 2 (d, e, f). Note: Location 1 and 2 are shown in Figure 1. A description of the
431 Manning's n values (N₁ to N₆) can be found in Table 2.

432



433

434 Figure 4. Change in simulated maximum flood inundation extents for (a) initial water
 435 depth, (b) Manning's n value, and (c) bathymetry correction factor.

436 3.3. Flood Model Evaluation

437 Because of a lack of observed streamflow data in the CRW, the performance of
 438 TRITON was evaluated by comparing the simulated 1% AEP flood map with the
 439 published 1% AEP flood map from FEMA (FEMA, 2019). The purpose of this
 440 assessment is to understand whether TRITON can provide comparable results to the
 441 widely accepted FEMA flood estimates. While the FEMA AEP flood maps do not
 442 necessarily represent complete ground truth, such a comparison is the best option given
 443 the data challenge. Similar approach has been utilized by several previous studies in the



444 evaluation of large- scale flood inundation evaluation (Alfieri et al., 2014; Wing et al.,
445 2017; Zheng et al., 2018; Gangrade et al., 2019).

446 To derive the 1% AEP flood map using TRITON, the ensemble-based approach used
447 by Gangrade et al. (2019) was followed. The assessment started by preparing the
448 streamflow hydrographs used to construct the 1% AEP flood map. The 1981–2012
449 annual maximum peak events and their corresponding 10-day streamflow hydrographs
450 were extracted from the control simulation. These streamflow hydrographs were then
451 proportionally rescaled to match the 1% AEP peak discharge estimated at the watershed
452 outlet (Figure 1), following the frequency analysis procedures outlined in Bulletin 17C
453 (England Jr. et al., 2019). The streamflow hydrographs from control simulations were
454 used for the peak discharge frequency analysis.

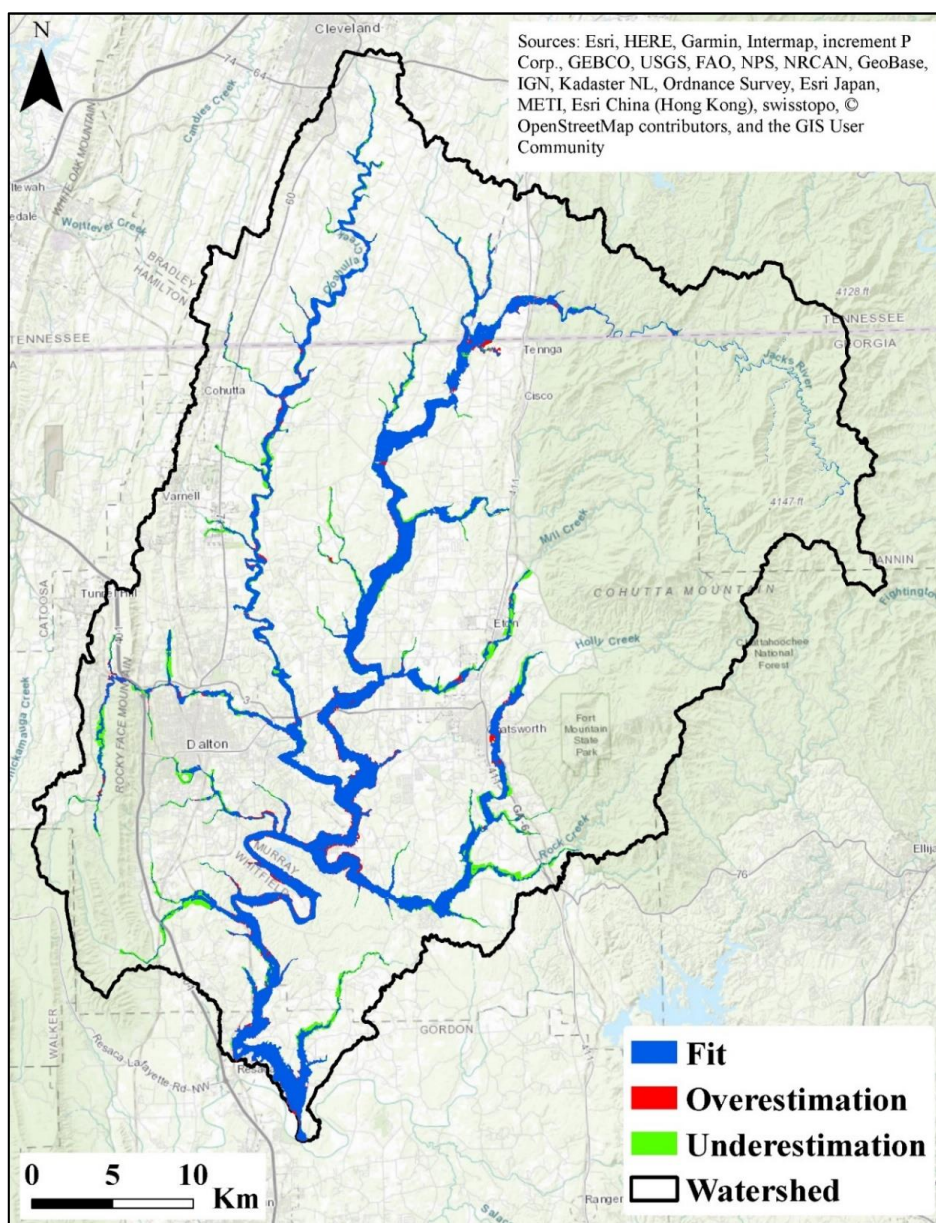
455 The results reported in the sensitivity analysis were also used to help identify suitable
456 TRITON parameters. In addition to streamflow hydrographs, TRITON requires DEM,
457 initial water depth, and Manning’s n value. To minimize the effect of bathymetric error in
458 the base DEM (Bhuyian et al., 2014; Bhuyian et al., 2019), we reduced the elevation
459 along the main channel by 0.15 m (i.e., a bathymetry correction factor). Although this
460 simple approach is unlikely to adjust the channel bathymetry to its true values, it can
461 improve the channel conveyance volume that is lost in the base DEM. To further improve
462 the quality of the base DEM, we removed elevated roads and bridges that could obstruct
463 the flow of water in some of the streams and rivers. An initial water depth of 0.35 m was
464 also selected in this study. For the surface roughness, a couple of flood simulations were
465 performed by adjusting the Manning’s n values for the main channel and floodplain to
466 achieve satisfactory agreement between the simulated and the reference FEMA flood



467 map. We eventually selected a single channel Manning's n value of 0.05 and a single
468 floodplain Manning's n value of 0.35.

469 Three evaluation metrics, including fit, omission, and commission (Kalyanapu et al.,
470 2011) were used to quantify the differences between the modeled and reference flood
471 map. The measure of fit determines the degree of relationship, while the omission and
472 commission statistically compare the simulated and reference FEMA flood maps
473 (Kalyanapu et al., 2011). The comparison between the simulated maximum inundation
474 and the corresponding 1% AEP FEMA flood map showed 80.65% fit, 5.52%
475 commission, and 15.36% omission (Figure 5), demonstrating that the TRITON could
476 reasonably estimate flood inundation extent, depths, and velocities in the CRW. The
477 computational efficiency of TRITON can further support ensemble inundation modeling
478 to provide additional variability information that cannot be provided by the conventional
479 deterministic flood map.

480



481

482 Figure 5. Comparison of simulated maximum flood extent with the corresponding FEMA

483 1% AEP flood map for the Conasauga River Watershed. Background layer source: ©

484 OpenStreetMap contributors 2020. Distributed under a Creative Commons BY-SA

485 License.

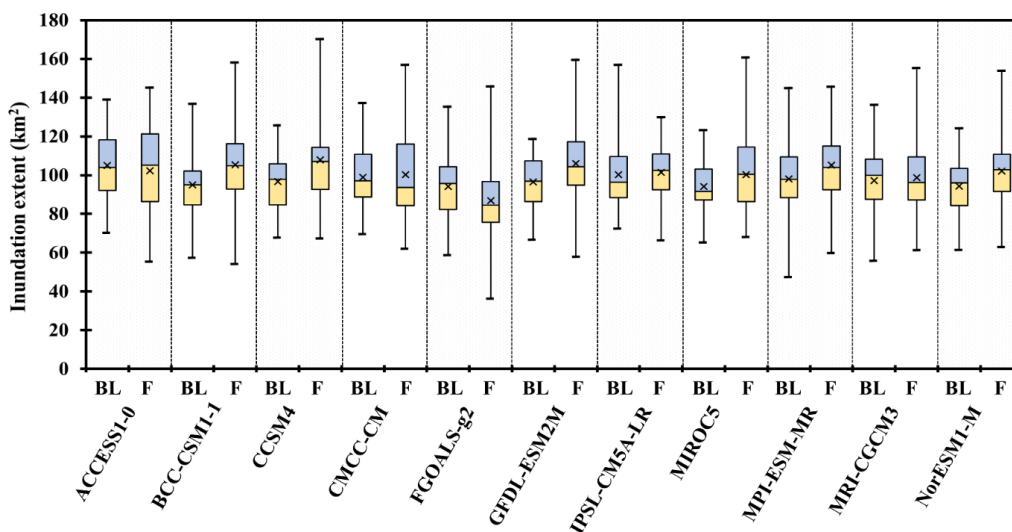


486

487 **3.4. Change in Flood Regime**

488 In this section, the projected changes in flood regime were calculated using the
489 flooded area from the baseline and future simulations for each ensemble member. Figure
490 6 illustrates the box and whisker plots for each of the 11 dynamically downscaled GCMs.
491 Given the small sample size in each distribution (40 compared to 440 in Figure 2), the
492 whiskers extend the largest/smallest data points with no outlier detection. For 9 out of the
493 11 downscaled climate models, the mean of 40 flood inundation showed an increase in
494 the floodplain area in the future period. In terms of the 75th percentile and maximum, 10
495 out of 11 models showed increase in the floodplain area. The distribution of maximum
496 future inundation of 4 models are found to be statistically different than their baseline
497 distributions at a 5% significance level. Note that the spread in the future period is
498 generally larger than the spread in the baseline period, suggesting an increase in the
499 hydrologic variability in the future period. Also, while the results from different models
500 were generally consistent, some inter-model differences were noted, which highlight the
501 need of a multi-model framework to capture the uncertainty in the future climate
502 projections. The multi-model approach provides a range of possible flood inundation
503 extents, which is critical for floodplain management decision making. The potential
504 increase in the floodplain area also demonstrates the importance of incorporating climate
505 change projections in the floodplain management regulations.

506



507

508 Figure 6. A summary of simulated maximum flood inundation extents obtained from the
509 baseline and future scenarios. The mean flooded area values are shown by × symbols.

510 Note: The suffix “_BL” represents baseline scenarios and the suffix “_F” represents
511 future scenarios.

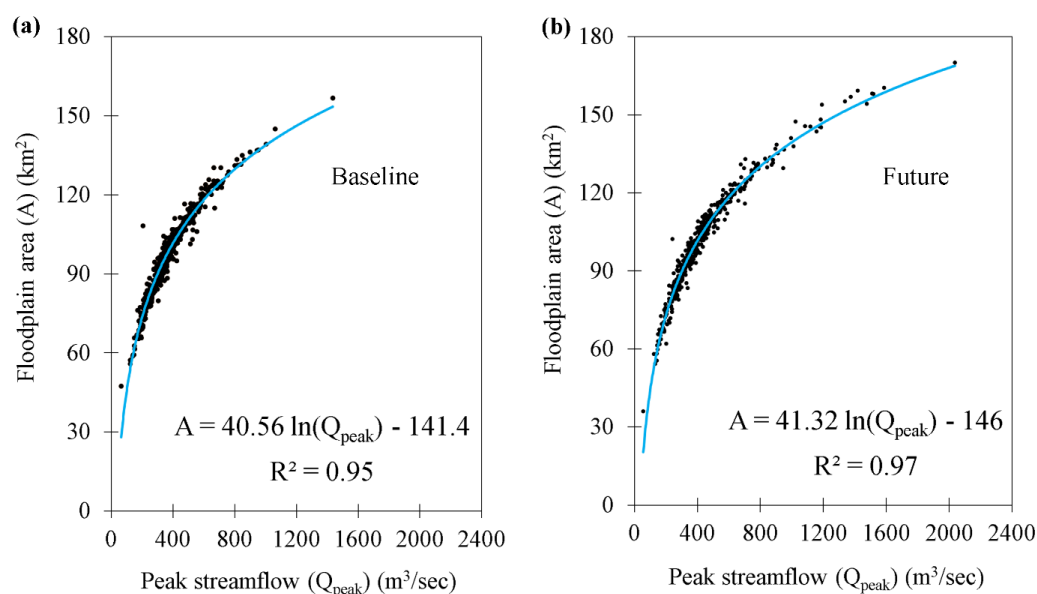
512 3.5. Flood Inundation Frequency Curve and Map

513 Figure 7 shows the relationship between the 440 flooded area values (across 11
514 downscaled GCMs) and their corresponding peak streamflow at the watershed outlet, for
515 both the baseline and future periods. Overall, both results (Figure 7a and 7b) exhibit
516 strong nonlinear relationships with high R^2 values. The results suggest that peak
517 streamflow is a significant variable controlling the total flooded area, but the variability
518 of flooded area could not be explained by peak streamflow alone. For instance, in the
519 baseline period, the peak streamflow values of 423.63 m³/sec and 424.25 m³/sec
520 correspond to 106.85 km² and 94.89 km² floodplain areas, respectively (Figure 7a).



521 Similarly, in the future period, the peak streamflow values of 433.27 m³/sec and 434.21
522 m³/sec correspond to 110.76 km² and 99.26 km² floodplain areas (Figure 7b).

523



524

525 Figure 7. Relationship between floodplain areas and peak streamflow values at the
526 watershed outlet for (a) baseline and (b) future scenarios. The blue lines indicate the
527 logarithmic best-fit.

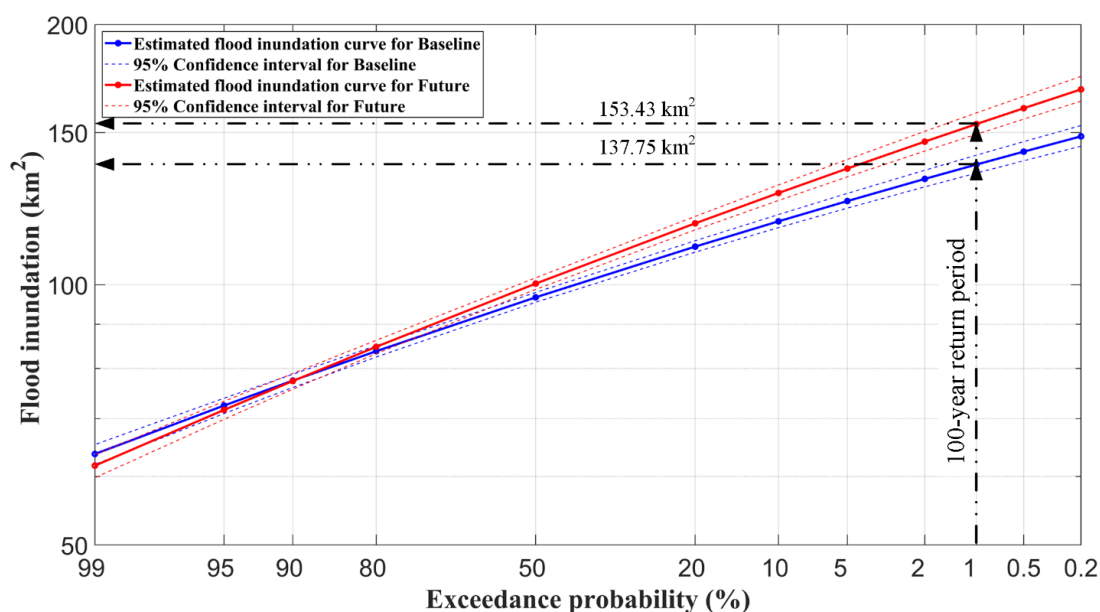
528

529 Figure 8 shows the event-based flood inundation frequency curves and their
530 corresponding 95% confidence intervals in both the baseline and future periods, for
531 which each frequency curve was derived using an ensemble of 440 years of data. The use
532 of long-term data helped reduce the uncertainty and add more confidence in the
533 evaluation of the lower AEP estimates. This type of assessment cannot be achieved using
534 only historic streamflow observations, for which the limited records present a major



535 challenge for lower AEP estimates. For most of the exceedance probabilities, the flooded
536 areas projected an increase in the inundation areas in the future period when compared to
537 the baseline period. The 1% AEP flood shows an $\sim 16 \text{ km}^2$ increase in the inundation area
538 (137.75 km^2 in the baseline period versus 153.43 km^2 in the future period) (Figure 8).
539 Similar results can be observed in inundation frequency curves developed for other AEPs
540 (not shown).

541



542

543 Figure 8. A summary of flood inundation frequency curves for the baseline and future
544 periods.

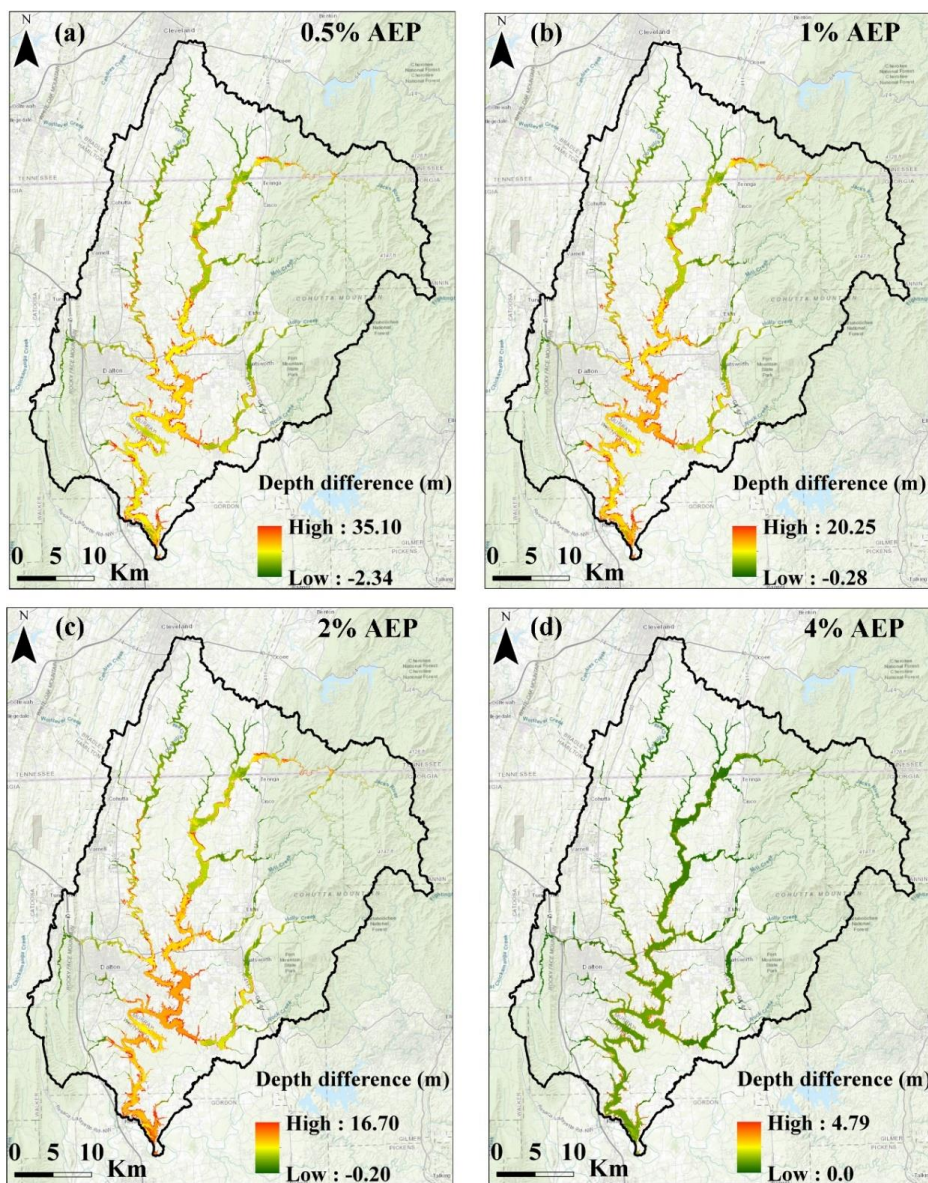
545

546 The grid-based flood depth frequency results at 0.5%, 1%, 2%, and 4% AEP levels
547 are illustrated in Figure 9. In each panel, the projected change (i.e., future minus baseline)
548 at each grid is shown. The corresponding histogram across the entire study area is

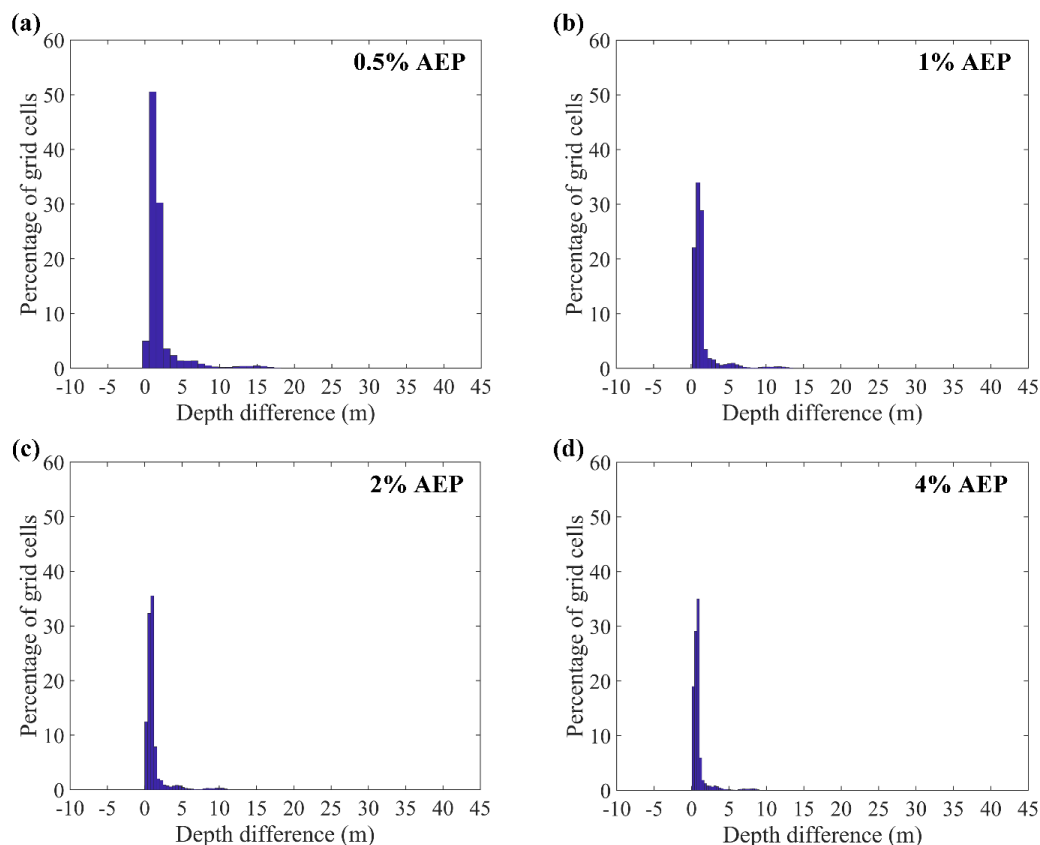


549 presented in Figure 10. Based on these comparisons, it is estimated that the flood depth
550 values at ~80% of grid cells would increase by 0.2 to 1.5 m due to projected changes in
551 climate (Figure 10). For 0.5% and 1% AEP flood depth frequency maps (Figure 9a and
552 9b), the changes in flood depth were more pronounced in the lower part of the CRW, near
553 the City of Dalton (where there are large population settlements), thereby increasing the
554 likelihood of population exposure to flood risk in the future period. Furthermore, for the
555 1% flood depth frequency map (Figure 9b), the projected increase in flood depths and
556 spatial extent has the potential to extend the flood damage far beyond the FEMA's
557 current base floodplain area. Therefore, these results highlight the need for climate
558 change consideration in the floodplain mapping. The approach presented in this study can
559 provide an alternative floodplain delineation technique, as it can be applied to develop
560 flood depth frequency maps that are reflective of the future climate.

561



562
563 Figure 9. Projected change (future minus baseline period) in flood depth frequency maps
564 for (a) 0.5%, (b) 1%, (c) 2%, and (d) 4% AEPs. ArcGIS background layer sources: ESRI,
565 HERE, Garmin, Intermap, GEBCO, USGS, Food and Agriculture Organization, National
566 Park Service, Natural Resources Canada, GeoBase, IGN, Kadaster NL, Ordnance Survey,
567 METI, Esri Japan, Esri China, the GIS User Community, and © OpenStreetMap
568 contributors 2020. Distributed under a Creative Commons BY-SA License.



569

570 Figure 10. Histograms for the future changes (2011–2050) in the flood depth relative to
571 the baseline period (1966–2005) for (a) 0.5%, (b) 1%, (c) 2%, and (d) 4% AEP flood
572 depth frequency maps.

573

574 3.6. Vulnerability of Electricity Infrastructure

575 Figure 11a shows the box and whisker plot for the distributions of maximum flood
576 depth values extracted at the substation location across all the baseline and future
577 simulations, assuming that no flood protection measures were adopted (mitigation
578 scenario 1). Of the 44 substations, 5 substations could have been affected during the

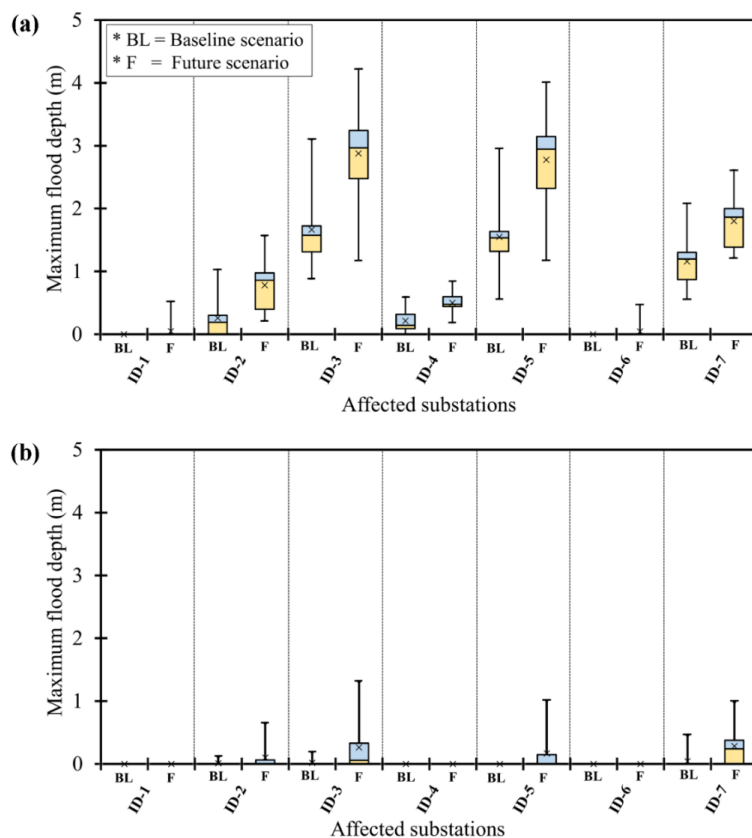


579 baseline period, while 7 substations are projected to be affected during the future period
580 (Figure 11a). Increases are indicated not only for the number of affected substations but
581 also for flood inundation depth values in the projected future climate. Overall, the mean
582 of the ensemble flood depth values shows an ~0.6 m increase in the future period (Figure
583 11a). Such an increase in the flood depth magnitude has the potential to exacerbate flood
584 related damage to electrical components, which can inflate the cost of hardening
585 measures such as elevating substations and constructing flood-protective barriers. As
586 expected, when the substations were flood-proofed up to BFE plus ~0.91 m (mitigation
587 scenario 2), the number of affected substations is reduced to three and four during the
588 baseline and future periods, respectively (Figure 11b). The locations of substations that
589 were impacted in the baseline period, in both mitigation scenarios, are consistent with the
590 Whitfield County Emergency Management Agency report map (EMA, 2016) that shows
591 the locations of critical facilities vulnerable to the historical flooding.

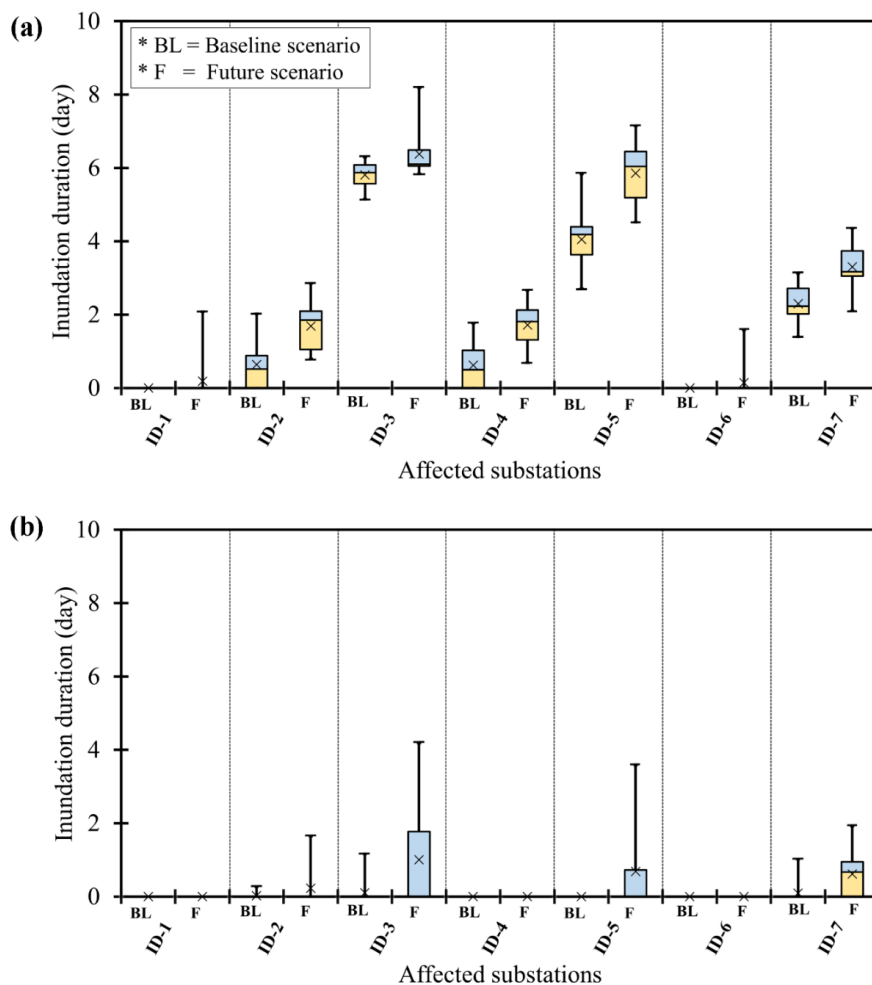
592 The maximum inundation durations at the affected substations are summarized in
593 Figure 12a (mitigation scenario 1) and Figure 12b (mitigation scenario 2). For both
594 mitigation scenarios and all affected substations, ensemble mean inundation durations
595 exhibited an increase under future climate condition. This increase in inundation duration
596 probably would render substations out of service for longer periods of time by making it
597 difficult to repair damaged substation equipment and restore grid services to customers.
598 The potential hazards and consequences may also extend to critical facilities that are
599 supplied by the affected substations. Similar to results presented in the previous sections,
600 these results demonstrate the need for improving existing flood mitigation measures by
601 incorporating the trends and uncertainties that originate from climate change. The



602 vulnerability analysis approach presented in this study will better equip floodplain
603 managers to identify the most vulnerable substations and to recommend suitable
604 adaptation measures, while allocating resources efficiently.



605
606 Figure 11. A summary of maximum flood depths for substations that were affected in the
607 baseline and/or future periods (a) without flood protection measures and (b) with flood
608 protection measures. Note: Affected substations with their corresponding IDs are shown
609 in Figure 1. There are no negative values in the vertical axis, as the minimum flood depth
610 value is zero.



611

612 Figure 12. A summary of maximum inundation durations for substations that were
 613 affected in the baseline and/or future periods (a) without flood protection measures and
 614 (b) with flood protection measures. Note: Affected substations with their corresponding
 615 IDs are shown in Figure 1. There are no negative values in the vertical axis, as the
 616 minimum inundation duration is zero.

617



618 **4. Summary and Conclusion**

619 This paper applies an integrated modeling framework to evaluate climate change
620 impacts on flood regime, floodplain protection standards, and electricity infrastructures
621 across the Conasauga River Watershed in the southeastern United States. Our evaluation
622 is based on a climate-hydrologic-hydraulic modeling framework, which makes use of an
623 eleven member ensemble of downscaled climate simulations. Nine out of eleven
624 ensemble members project an increase in the flood inundation area in the future period.
625 Similarly, at the 1% AEP level, the flood inundation frequency curves indicate $\sim 16 \text{ km}^2$
626 increase in floodplain area under the future climate. The comparison between the flood
627 depth frequency maps from the baseline and future simulations indicated that, on average,
628 $\sim 80\%$ of grid cells exhibit a 0.2 to 1.5 m increase in the flood depth values. Without the
629 flood protection measures, of the 44 electric substations inside the watershed, 5 and 7
630 substations could be affected during the baseline and future periods, respectively. Even
631 after flood-proofing, three and four substations could still be affected in the baseline and
632 future periods. The increases in flood depth magnitude and inundation duration at the
633 affected substations in the future period will most likely damage more electrical
634 components, inflate the cost of hardening measures and render substations out of service
635 for a longer period of time.

636 Although future climate conditions are uncertain, our results demonstrate the needs
637 for (1) consideration of climate change in the floodplain management regulations; (2)
638 improvements in the conventional deterministic flood delineation approach through the
639 inclusion of probabilistic or ensemble-based methods, and (3) improvements in the
640 existing flood protection measures for critical electricity infrastructures through enhanced



641 hydro-meteorologic modeling capacities. In particular, rapidly advanced high-
642 performance computing capabilities have enabled the incorporation of computationally
643 intensive 2D hydraulics modeling in the ensemble-based hydroclimate impact
644 assessment. While the computational cost demonstrated in this study may still seem
645 steep, in the current speed of technology advancement, we will soon be able to implement
646 such a computationally intensive assessment for wide applications. The approach
647 presented in this study can be used by floodplain managers to develop flood depth
648 frequency maps and to identify the most vulnerable electric substations.

649 **Author Contribution**

650 *Dullo, Kalyanapu, Kao, Gangrade* and *Morales-Hernández* developed the concept for the
651 paper, designed the methodology and *Dullo* performed all the simulations required for the
652 study with feedback from all the co-authors. *Sharif, Ghafoor* and *Morales-Hernández*
653 focused on programming, software development and testing of existing code components.
654 *Ashfaq* and *Morales-Hernández* provided access to supercomputing machine hours on
655 ORNL's SUMMIT and RHEA computers. The manuscript was edited by *Dullo* with inputs
656 from the co-authors.

657 **Competing Interests**

658 The authors declare that they have no conflict of interest.

659 **Acknowledgments**

660 This study was supported by the US Air Force Numerical Weather Modeling
661 Program. TTD, MBS, AJK, and SG also acknowledge support by the Center of
662 Management, Utilization, and Protection of Water Resources at Tennessee Technological
663 University. Some portion of the project was funded by the UT Battelle Subcontract No:



664 4000164401. The research used resources of the Oak Ridge Leadership Computing
665 Facility at Oak Ridge National Laboratory. Some of the co-authors are employees of UT-
666 Battelle LLC under contract DE-AC05-00OR22725 with the US Department of Energy.
667 Accordingly, the US government retains and the publisher, by accepting the article for
668 publication, acknowledges that the US government retains a nonexclusive, paid-up,
669 irrevocable, worldwide license to publish or reproduce the published form of this
670 manuscript, or allow others to do so, for US government purposes. The input data sets are
671 cited throughout the paper, as appropriate.

672 **Data Availability**

673 The data that support the findings of this study are openly available in figshare
674 repository at the following URL:

675 https://figshare.com/projects/Conasauga_Flood_Modeling_Project/80840.

676 **References**

677 AECOM: The Impact of Climate Change and Population Growth on the National Flood

678 Insurance Program through 2100, available at: [https://www.aecom.com/content/wp-](https://www.aecom.com/content/wp-content/uploads/2016/06/Climate_Change_Report_AECOM_2013-06-11.pdf)
679 [content/uploads/2016/06/Climate_Change_Report_AECOM_2013-06-11.pdf](https://www.aecom.com/content/uploads/2016/06/Climate_Change_Report_AECOM_2013-06-11.pdf) (last

680 access: 12 October 2019), 2013.

681 Alfieri, L., Salamon, P., Bianchi, A., Neal, J., Bates, P., and Feyen, L.: Advances in Pan-

682 European Flood Hazard Mapping, *Hydrol. Process.*, 28(13), 4067–4077,

683 doi:10.1002/hyp.9947, 2014.

684 Alfieri, L., Burek, P., Feyen, L., and Forzieri, G.: Global Warming Increases the

685 Frequency of River Floods in Europe, *Hydrol. Earth Syst. Sci.*, 19, 2247–2260,

686 doi:10.5194/hess-19-2247-2015, 2015a.



- 687 Alfieri, L., Feyen, L., Dottori, F., and Bianchi, A.: Ensemble Flood Risk Assessment in
688 Europe Under High End Climate Scenarios, *Global Environ. Chang.*, 35, 199–212,
689 doi:10.1016/j.gloenvcha.2015.09.004, 2015b.
- 690 Alfieri, L., Bisselink, B., Dottori, F., Naumann, G., de Roo, A., Salamon, P., Wyser, K.,
691 and Feyen, L.: Global Projections of River Flood Risk in a Warmer World, *Earth's*
692 *Future*, 5, 171–182, doi:10.1002/2016EF000485, 2017.
- 693 Alfieri, L., Dottori, F., Betts, R., Salamon, P., and Feyen, L.: Multi-Model Projections of
694 River Flood Risk in Europe under Global Warming, *Climate*, 6(6),
695 doi:10.3390/cli6010006, 2018.
- 696 Allen-Dumas, M. R., Binita, K. C., and Cunliff, C. I.: Extreme Weather and Climate
697 Vulnerabilities of the Electric Grid: A Summary of Environmental Sensitivity
698 Quantification Methods, ORNL/TM-2019/1252, Oak Ridge National Laboratory,
699 available at: [https://www.energy.gov/sites/prod/files/2019/09/f67/
700 \[Oak%20Ridge%20National%20Laboratory%20EIS%20Response.pdf\]\(https://www.energy.gov/sites/prod/files/2019/09/f67/Oak%20Ridge%20National%20Laboratory%20EIS%20Response.pdf\) \(last access: 17
701 December 2019\), 2019.](https://www.energy.gov/sites/prod/files/2019/09/f67/Oak%20Ridge%20National%20Laboratory%20EIS%20Response.pdf)
- 702 Archuleta, C.-A. M., Constance, E. W., Arundel, S. T., Lowe, A. J., Mantey, K. S., and
703 Phillips, L. A.: The National Map Seamless Digital Elevation Model Specifications,
704 US Geological Survey Techniques and Methods 11-B9, doi:10.3133/tm11B9,
705 available at: <https://pubs.er.usgs.gov/publication/tm11B9> (last access: 31 December
706 2019), 2017.
- 707 Arnell, N. W. and Gosling, S. N.: The Impacts of Climate Change on River Flood Risk at
708 the Global Scale, *Clim. Change*, 134, 387–401, doi:10.1007/s10584-014-1084-5,
709 2014.



- 710 Ashfaq, M., Bowling, L. C., Cherkauer, K., Pal, J. S., and Diffenbaugh, N. S.: Influence
711 of Climate Model Biases and Daily-scale Temperature and Precipitation Events on
712 Hydrological Impacts Assessment: A Case Study of the United States, *J. Geophys.*
713 *Res.*, 115, D14116, doi:10.1029/2009JD012965, 2010.
- 714 Ashfaq, M., Ghosh, S., Kao, S.-C., Bowling, L. C., Mote, P., Touma, D., Rauscher, S. A.,
715 and Diffenbaugh, N. S.: Near-term Acceleration of Hydroclimatic Change in the
716 Western U.S., *J. Geophys. Res.*, 118, 10,676–10,693, doi:10.1002/jgrd.50816, 2013.
- 717 Ashfaq, M., Rastogi, D., Mei, R., Kao, S.-C., Gangrade, S., Naz, B. S., and Touma, D.:
718 High-resolution Ensemble Projections of Near-term Regional Climate over the
719 Continental United States. *J. Geophys. Res.*, 121, 9943–9963,
720 doi:10.1002/2016JD025285, 2016.
- 721 Baechler, M. C., Gilbride, T. L., Cole, P. C., Hefty, M. G., and Ruiz, K.: Building
722 America Best Practices Series, Volume 7.3, High-Performance Home Technologies:
723 Guide to Determining Climate Regions by County, Pacific Northwest National
724 Laboratory, US Department of Energy under Contract DE-AC05-76RLO 1830,
725 PNNL-17211 Rev. 3, available at:
726 https://www.energy.gov/sites/prod/files/2015/10/f27/ba_climate_region_guide_7.3.pdf
727 [f](#) (last access: 27 September 2020), 2015.
- 728 Bhuyian, Md. N. M., Kalyanapu, A. J., and Nardi, F.: Approach to Digital Elevation
729 Model Correction by Improving Channel Conveyance, *J. Hydrol. Eng.*, 20(5),
730 doi:10.1061/(ASCE)HE.1943-5584.0001020, 2014.
- 731 Bhuyian, Md. N. M., Dullo, T. T., Kalyanapu, A. J., Gangrade, S., and Kao, S.-C.:
732 Application of Geomorphic Correlations for River Bathymetry Correction in Two-



- 733 dimensional Hydrodynamic Modeling for Long-term Flood Risk Evaluation, World
734 Environmental and Water Resources Congress, Pittsburgh, Pennsylvania, USA, 19-23
735 May 2019, 2019.
- 736 Birhanu, D., Kim, H., Jang, C., and Park, S.: Flood Risk and Vulnerability of Addis
737 Ababa City Due to Climate Change and Urbanization, *Procedia Engineer.*, 154, 696–
738 702, doi:10.1016/j.proeng.2016.07.571, 2016.
- 739 Blessing, R., Sebastian, A., and Brody, S. D.: Flood Risk Delineation in the United
740 States: How Much Loss Are We Capturing?, *Nat. Hazards Rev.*, 18(3), 04017002-(1-
741 10), doi:10.1061/(ASCE)NH.1527-6996.0000242, 2017.
- 742 Bollinger, L. A. and Dijkema, G. P. J.: Evaluating Infrastructure Resilience to Extreme
743 Weather – the Case of the Dutch Electricity Transmission Network, *EJTIR*, 16(1),
744 214–239, doi:10.18757/ejtir.2016.16.1.3122, 2016.
- 745 Bragatto, T., Cresta, M., Cortesi, F., Gatta, F. M., Geri, A., Maccioni, M., and Paulucci,
746 M.: Assessment and Possible Solution to Increase Resilience: Flooding Threats in
747 Terni Distribution Grid, *Energies*, 12(4), 744, doi:10.3390/en12040744, 2019.
- 748 Brunner, G. W., Warner, J. C., Wolfe, B. C., Piper, S. S., and Marston, L.: Hydrologic
749 Engineering Center – River Analysis System (HEC-RAS) Applications Guide 2016,
750 Version 5.0, US Army Corps of Engineers, CA, available at:
751 <https://www.hec.usace.army.mil/software/hec-ras/documentation/HEC->
752 [RAS%205.0%20Applications%20Guide.pdf](https://www.hec.usace.army.mil/software/hec-ras/documentation/HEC-RAS%205.0%20Applications%20Guide.pdf) (last access: 27 December 2019), 2016.
- 753 Burkey, J.: Log-Pearson Flood Flow Frequency using USGS 17B, available at:
754 <https://www.mathworks.com/matlabcentral/fileexchange/22628-log-pearson-flood->
755 [flow-frequency-using-usgs-17b](https://www.mathworks.com/matlabcentral/fileexchange/22628-log-pearson-flood-flow-frequency-using-usgs-17b) (last access: 23 December 2019), 2009.



- 756 Chandramowli, S. N. and Felder, F. A.: Impact of Climate Change on Electricity Systems
757 and Markets – A Review of Models and Forecasts, *Sustain. Energy Technol. Assess.*,
758 5, 62–74, doi:10.1016/j.seta.2013.11.003, 2014.
- 759 Ciscar, J. C. and Dowling, P.: Integrated Assessment of Climate Impacts and Adaptation
760 in the Energy Sector, *Energy Econ.*, 46, 531–538, doi:10.1016/j.eneco.2014.07.003,
761 2014.
- 762 Cronin, J., Anandarajah, G., and Dessens, O.: Climate Change Impacts on the Energy
763 System: A Review of Trends and Gaps, *Clim. Change*, 151, 79–93,
764 doi:10.1007/s10584-018-2265-4, 2018.
- 765 Daly, C., Halbleib, M., Smith, J. I., Gibson, W. P., Doggett, M. K., Taylor, G. H., Curtis,
766 J., and Pasteris, P. P.: Physiographically Sensitive Mapping of Climatological
767 Temperature and Precipitation Across the Conterminous United States, *Int. J.*
768 *Climatol.*, 28(15), 2031–2064, doi:10.1002/joc.1688, 2008.
- 769 Elliott, K. J. and Vose, J. M.: Initial Effects of Prescribed Fire on Quality of Soil Solution
770 and Streamwater in the Southern Appalachian Mountains, *South. J. Appl. For.*, 29(1),
771 5–15, doi:10.1093/sjaf/29.1.5, 2005.
- 772 Elsner, M. M., Cuo, L., Voisin, N., Deems, J. S., Hamlet, A. F., Vano, J. A., Mickelson,
773 K. E. B., Lee, S.-Y., and Lettenmaier, D. P.: Implications of 21st Century Climate
774 Change for the Hydrology of Washington State, *Climatic Change*, 102(1–2), 225–
775 260, doi:10.1007/s10584-010-9855-0, 2010.
- 776 EMA (Emergency Management Agency): Whitfield County Hazard Mitigation Plan
777 2016, Including the Cities of Dalton, Tunnel Hill, and Varnell, and the Town of
778 Cohutta, Whitfield County Emergency Management Agency, available at:



779 <https://www.whitfieldcountyga.com/ema/WhitfieldHMPDraft52616.pdf> (last access:
780 29 March 2020), 2016.

781 England Jr., J. F., Cohn, T. A., Faber, B. A., Stedinger, J. R., Thomas Jr., W. O.,
782 Veilleux, A. G., Kiang, J. E., and Mason Jr., R. R.: Guidelines for Determining Flood
783 Flow Frequency—Bulletin 17C, Techniques and Methods 4-B5, US Geological
784 Survey, <https://doi.org/10.3133/tm4B5>, 2019.

785 Farber-DeAnda, M., Cleaver, M., Lewandowski, C., and Young, K.: Hardening and
786 Resiliency: US Energy Industry Response to Recent Hurricanes Seasons, Office of
787 Electricity Delivery and Energy Reliability, US Department of Energy, available at:
788 <https://www.oe.netl.doe.gov/docs/HR-Report-final-081710.pdf> (last access: 17
789 December 2019), 2010.

790 FEMA (Federal Emergency Management Agency): National Flood Insurance Program:
791 Program Description, Federal Emergency Management Agency, available at:
792 [https://www.fema.gov/media-library-data/20130726-1447-20490-
793 2156/nfipdescrip_1_.pdf](https://www.fema.gov/media-library-data/20130726-1447-20490-2156/nfipdescrip_1_.pdf) (last access: 22 January 2018), 2002.

794 FEMA (Federal Emergency Management Agency): Emergency Power Systems for
795 Critical Facilities: A Best Practices Approach to Improving Reliability, FEMA P-
796 1019, Applied Technology Council, Redwood City, CA, available at:
797 <https://www.fema.gov/media-library/assets/documents/101996> (last access: 17
798 December 2019), 2014.

799 FEMA (Federal Emergency Management Agency): FEMA Flood Map Service Center,
800 available at: <https://msc.fema.gov/portal/availabilitySearch?#searchresultsanchor>
801 (last access: 28 December 2019), 2019.



802 FIS (Flood Insurance Study): Flood Insurance Study: Whitfield County, Georgia and
803 Incorporated Areas, Flood Insurance Study Number: 13313CV000A, Federal
804 Emergency Management Agency, available at: [http://www.georgiadfirm.com/pdf/](http://www.georgiadfirm.com/pdf/panels/13313CV000A.pdf)
805 [panels/13313CV000A.pdf](http://www.georgiadfirm.com/pdf/panels/13313CV000A.pdf) (last access: 25 December 2019), 2007.

806 FIS (Flood Insurance Study): Flood Insurance Study: Murray County, Georgia and
807 Incorporated Areas, Flood Insurance Study Number: 13213CV000A, Federal
808 Emergency Management Agency, available at:
809 <http://www.georgiadfirm.com/pdf/panels/13213CV000A.pdf> (last access: 27
810 December 2019), 2010.

811 Forzieri, G., Bianchi, A., e Silva, F. B., Herrera, M. A. M., Leblois, A., Lavallo, C.,
812 Aerts, J. C. J. H., and Feyen, L.: Escalating Impacts of Climate Extremes on Critical
813 Infrastructures in Europe, *Glob. Environ. Change*, 48, 97–107,
814 doi:10.1016/j.gloenvcha.2017.11.007, 2018.

815 Fu, G., Wilkinson, S., Dawson, R. J., Fowler, H. J., Kilsby, C., Panteli, M., and
816 Mancarella, P.: Integrated Approach to Assess the Resilience of Future Electricity
817 Infrastructure Networks to Climate Hazards, *IEEE Syst. J.*, 12(4), 3169–3180,
818 doi:10.1109/JSYST.2017.2700791, 2017.

819 Galloway, G. E., Baecher, G. B., Plasencia, D., Coulton, K. G., Louthain, J., Bagha, M.,
820 and Levy, A. R.: Assessing the Adequacy of the National Flood Insurance Program’s
821 1 Percent Flood Standard, Water Policy Collaborative, University of Maryland,
822 available at: <https://www.fema.gov/media-library/assets/documents/9594> (last access:
823 17 December 2019), 2006.



- 824 Gangrade, S., Kao, S.-C., Naz, B. S., Rastogi, D., Ashfaq, M., Singh, N., and Preston, B.
825 L.: Sensitivity of Probable Maximum Flood in a Changing Environment, *Water*
826 *Resour. Res.*, 54(6), 3913–3936, doi:10.1029/2017WR021987, 2018.
- 827 Gangrade, S., Kao, S.-C., Dullo, T. T., Kalyanapu, A. J., and Preston, B. L.: Ensemble-
828 based Flood Vulnerability Assessment for Probable Maximum Flood in a Changing
829 Environment, *J. Hydrol.*, 576, 342–355, doi:10.1016/j.jhydrol.2019.06.027, 2019.
- 830 Gangrade, S., Kao, S.-C., and McManamay, R. A.: Multi-model Hydroclimate
831 Projections for the Alabama-Coosa-Tallapoosa River Basin in the Southeastern
832 United States, *Sci. Rep.*, 10, 2870, doi:10.1038/s41598-020-59806-6, 2020.
- 833 Gilstrap, M., Amin, S., and DeCorla-Souza, K.: United States Electricity Industry Primer,
834 DOE/OE-0017, Office of Electricity Delivery and Energy Reliability, US Department
835 of Energy, Washington DC, available at:
836 [https://www.energy.gov/sites/prod/files/2015/12/f28/united-states-electricity-
837 industry-primer.pdf](https://www.energy.gov/sites/prod/files/2015/12/f28/united-states-electricity-
837 industry-primer.pdf) (last access: 17 December 2019), 2015.
- 838 Giorgi, F., Coppola, E., Solmon, F., Mariotti, L., Sylla, M. B., Bi, X., Elguindi, N., Diro,
839 G. T., Nair, V., Giuliani, G., Turuncoglu, U. U., Cozzini, S., Güttler, I., O'Brien, T.
840 A., Tawfik, A. B., Shalaby, A., Zakey, A. S., Steiner, A. L., Stordal, F., Sloan, L. C.,
841 and Brankovic, C.: RegCM4: model description and preliminary tests over multiple
842 CORDEX domains, *Climate Res.*, 52, 7–29, doi:10.3354/cr01018, 2012.
- 843 HCFCFD (Harris County Flood Control District): Hurricane Harvey – Storm and Flood
844 Information, available at: [https://www.hcfcfd.org/Portals/62/Harvey/immediate-flood-
845 report-final-hurricane-harvey-2017.pdf](https://www.hcfcfd.org/Portals/62/Harvey/immediate-flood-
845 report-final-hurricane-harvey-2017.pdf) (last access: 16 December 2019), 2018.



- 846 HIFLD (Homeland Infrastructure Foundation-Level Data): Homeland Infrastructure
847 Foundation-Level Data, Electric Substations, US Department of Homeland Security,
848 available at: [https://hifld-geoplatform.opendata.arcgis.com/datasets/electric-](https://hifld-geoplatform.opendata.arcgis.com/datasets/electric-substations)
849 [substations](https://hifld-geoplatform.opendata.arcgis.com/datasets/electric-substations) (last access: 20 December 2019), 2019.
- 850 Hirabayashi, Y., Mahendran, R., Koirala, S., Konoshima, L., Yamazaki, D., Watanabe,
851 S., Kim, H., and Kanae, S.: Global Flood Risk under Climate Change, *Nature Clim.*
852 *Chang.*, 3, 816–821, doi:10.1038/NCLIMATE1911, 2013.
- 853 Hou, Z., Ren, H., Sun, N., Wigmosta, M. S., Liu, Y., Leung, L. R., Yan, H., Skaggs, R.,
854 and Coleman, A.: Incorporating Climate Nonstationarity and Snowmelt Processes in
855 Intensity–Duration–Frequency Analyses with Case Studies in Mountainous Areas, *J.*
856 *Hydrometeorol.*, 20(12), 2331–2346, doi:10.1175/JHM-D-19-0055.1, 2019.
- 857 Ivey, G. and Evans, K.: Conasauga River Alliance Business Plan: Conasauga River
858 Watershed Ecosystem Project, available at: [https://www.fs.fed.us/](https://www.fs.fed.us/largewatershedprojects/businessplans/)
859 [largewatershedprojects/businessplans/](https://www.fs.fed.us/largewatershedprojects/businessplans/) (last access: 22 December 2019), 2000.
- 860 Kalyanapu, A. J., Shankar, S., Pardyjak, E. R., Judi, D. R., and Burian, S. J.: Assessment
861 of GPU Computational Enhancement to a 2D Flood Model, *Environ. Modell. Softw.*,
862 26(8), 1009–1016, doi:10.1016/j.envsoft.2011.02.014, 2011.
- 863 Kefi, M., Mishra, B. K., Kumar, P., Masago, Y., and Fukushi, K.: Assessment of
864 Tangible Direct Flood Damage Using a Spatial Analysis Approach under the Effects
865 of Climate Change: Case Study in an Urban Watershed in Hanoi, Vietnam, *Int. J.*
866 *Geo-Inf.*, 7, 29, doi:10.3390/ijgi7010029, 2018.
- 867 Kollat, J. B., Kasprzyk, J. R., Thomas Jr., W. O., Miller, A. C., and Divoky, D.:
868 Estimating the Impacts of Climate Change and Population Growth on Flood



- 869 Discharges in the United States, *J. Water Resour. Plann. Manage.*, 138(5), 442–452,
870 doi:10.1061/(ASCE)WR.1943-5452.0000233, 2012.
- 871 Langerwisch, F., Rost, S., Gerten, D., Poulter, B., Rammig, A., and Cramer, W.: Potential
872 Effects of Climate Change on Inundation Patterns in the Amazon Basin, *Hydrol.*
873 *Earth Syst. Sci.*, 17, 2247–2262, doi:10.5194/hess-17-2247-2013, 2013.
- 874 Li, H., Sun, J., Zhang, H., Zhang, J., Jung, K., Kim, J., Xuan, Y., Wang, X., and Li, F.:
875 What Large Sample Size Is Sufficient for Hydrologic Frequency Analysis? – A
876 Rational Argument for a 30-Year Hydrologic Sample Size in Water Resources
877 Management, *Water*, 10, 430, doi:10.3390/w10040430, 2018.
- 878 Marshall, R., Ghafoor, S., Rogers, M., Kalyanapu, A., and Dullo, T. T.: Performance
879 Evaluation and Enhancements of a Flood Simulator Application for Heterogeneous
880 HPC Environments, *Int. J. Network Comput.*, 8(2), 387–407, 2018.
- 881 Mikellidou, C. V., Shakou, L. M., Boustras, G., and Dimopoulos, C.: Energy Critical
882 Infrastructures at Risk from Climate Change: A State of the Art Review, *Saf. Sci.*,
883 110, 110–120, doi:10.1016/j.ssci.2017.12.022, 2018.
- 884 Milly, P. C. D., Wetherald, R. T., Dunne, K. A., and Delworth, T. L.: Increasing Risk of
885 Great Floods in a Changing Climate, *Nature*, 415(6871), 514–517,
886 doi:10.1038/415514a, 2002.
- 887 Mora, C., Spirandelli, D., Franklin, E. C., Lynham, J., Kantar, M. B., Miles, W., Smith,
888 C. Z., Freel, K., Moy, J., Louis, L. V., Barba, E. W., Bettinger, K., Frazier, A. G.,
889 Colburn IX, J. F., Hanasaki, N., Hawkins, E., Hirabayashi, Y., Knorr, W., Little, C.
890 M., Emanuel, K., Sheffield, J., Patz, J. A., and Hunter, C. L.: Broad Threat to
891 Humanity from Cumulative Climate Hazards Intensified by Greenhouse Gas



- 892 Emissions, *Nature Clim. Chang.*, 8, 1062–1071, doi:10.1038/s41558-018-0315-6,
893 2018.
- 894 Morales-Hernández, M., Sharif, M. B., Gangrade, S., Dullo, T. T., Kao, S.-C.,
895 Kalyanapu, A., Ghafoor, S. K., Evans, K. J., Madadi-Kandjani, E., and Hodges, B. R.:
896 High Performance Computing in Water Resources Hydrodynamics, *Journal of*
897 *Hydroinformatics*, in press, 2020a.
- 898 Morales-Hernández, M., Sharif, Md. B., Kalyanapu, A., Ghafoor, S. K., Dullo, T.T.,
899 Gangrade, S., Kao, S.-C., Norman, M. R., and Evans, K. J.: TRITON: A Multi-GPU
900 Open Source 2D Hydrodynamic Flood, Submitted to *Environmental Modelling &*
901 *Software*, 2020b.
- 902 NERC (North American Electric Reliability Corporation): Hurricane Harvey Event
903 Analysis Report, North American Electric Reliability Corporation, Atlanta, GA,
904 available at: [https://www.nerc.com/pa/rmm/ea/Hurricane_Harvey_EAR_DL/](https://www.nerc.com/pa/rmm/ea/Hurricane_Harvey_EAR_DL/NERC_Hurricane_Harvey_EAR_20180309.pdf)
905 [NERC_Hurricane_Harvey_EAR_20180309.pdf](https://www.nerc.com/pa/rmm/ea/Hurricane_Harvey_EAR_20180309.pdf) (last access: 17 December 2019),
906 2018.
- 907 Ntelekos, A. A., Oppenheimer, M., Smith, J. A., and Miller, A. J.: Urbanization, Climate
908 Change and Flood Policy in the United States, *Clim. Chang.*, 103, 597–616,
909 doi:10.1007/s10584-009-9789-6, 2010.
- 910 Nyaupane, N., Thakur, B., Kalra, A., and Ahmad, S.: Evaluating Future Flood Scenarios
911 Using CMIP5 Climate Projections, *Water*, 10, 1866, doi:10.3390/w10121866, 2018.
- 912 Olsen, J. R.: Climate Change and Floodplain Management in the United States, *Clim.*
913 *Change*, 76, 407–426, doi:10.1007/s10584-005-9020-3, 2006.



- 914 Pachauri, R. K. and Meyer, L. A.: Intergovernmental Panel on Climate Change (IPCC):
915 Climate Change 2014: Synthesis Report, in Proceedings of Contribution of Working
916 Groups I, II and III to the Fifth Assessment Report of the Intergovernmental Panel on
917 Climate Change, Geneva, Switzerland, available at:
918 https://www.ipcc.ch/site/assets/uploads/2018/05/SYR_AR5_FINAL_full_wcover.pdf
919 (last access: 16 December 2019), 2014.
- 920 Pant, R., Thacker, S., Hall, J. W., Alderson, D., and Barr, S.: Critical Infrastructure
921 Impact Assessment Due to Flood Exposure, *J. Flood Risk Manag.*, 11, 22–33,
922 doi:10.1111/jfr3.12288, 2017.
- 923 Pielke Jr., R. A. and Downton, M. W.: Precipitation and Damaging Floods: Trends in the
924 United States, 1932–97, *J. Climate*, 13(20), 3625–3637, doi:10.1175/1520-
925 0442(2000)013<3625:PADFTI>2.0.CO;2, 2000.
- 926 Pielke Jr., R. A., Downton, M. W., and Barnard Miller, J. Z.: Flood Damage in the United
927 States, 1926–2000: A reanalysis of National Weather Service Estimates, National
928 Center for Atmospheric Research, Boulder, CO, available at:
929 <https://sciencepolicy.colorado.edu/flooddamagedata/flooddamagedata.pdf> (last
930 access: 16 December 2019), 2002.
- 931 Pralle, S.: Drawing Lines: FEMA and the Politics of Mapping Flood Zones, *Clim.*
932 *Chang.*, 152, 227–237, doi:10.1007/s10584-018-2287-y, 2019.
- 933 Reed, D. A., Kapur, K. C., and Christie, R. D.: Methodology for Assessing the Resilience
934 of Networked Infrastructure, *IEEE Syst. J.*, 3(2), 174–180,
935 doi:10.1109/JSYST.2009.2017396, 2009.



- 936 Storck, P., Bowling, L., Wetherbee, P., and Lettenmaier, D.: Application of a GIS-Based
937 Distributed Hydrology Model for Prediction of Forest Harvest Effects on Peak
938 Stream Flow in the Pacific Northwest, *Hydrol. Process.*, 12(6), 889–904,
939 doi:10.1002/(SICI)1099-1085(199805)12:6<889::AID-HYP661>3.0.CO;2-P, 1998.
- 940 Strauss, B. and Ziemiński, R.: Sea Level Rise Threats to Energy Infrastructure: A
941 Surging Seas Brief Report by Climate Central, Climate Central, Washington, DC,
942 available at: <http://slr.s3.amazonaws.com/SLR-Threats-to-Energy-Infrastructure.pdf>
943 (last access: 17 December 2019), 2012.
- 944 Tan, A.: Sandy and Its Impacts: Chapter 1, NYC Special Initiative for Rebuilding and
945 Resiliency, NYC Resources, NY, available at:
946 http://www.nyc.gov/html/sirr/downloads/pdf/final_report/Ch_1_SandyImpacts_FINAL_singles.pdf
947 (last access: 17 December 2019), 2013.
- 948 Thornton, P. E., Running, S. W., and White, M. A.: Generating surfaces of daily
949 meteorological variables over large regions of complex terrain, *J. Hydrol.*, 190, 214–
950 251, doi:10.1016/S0022-1694(96)03128-9, 1997.
- 951 UNISDR (United Nations Office for Disaster Risk Reduction): Making Development
952 Sustainable: The Future of Disaster Risk Management, Global Assessment Report on
953 Disaster Risk Reduction, Geneva, Switzerland, available at:
954 [https://www.preventionweb.net/english/hyogo/gar/2015/en/gar-
955 pdf/GAR2015_EN.pdf](https://www.preventionweb.net/english/hyogo/gar/2015/en/gar-pdf/GAR2015_EN.pdf) (last access: 16 December 2019), 2015.
- 956 USACE (US Army Corps of Engineers): Master Water Control Manual: Alabama-Coosa-
957 Tallapoosa (ACT) River Basin, Alabama, Georgia, US Army Corps of Engineers,
958 available at: <https://www.sam.usace.army.mil/Portals/46/docs/>



- 959 [planning_environmental/act/docs/New/ACT%20Master%20Manual_March%2013.pdf](#)
960 [f](#) (last access: 22 December 2019), 2013.
- 961 USGS (US Geological Survey): Guidelines for Determining Flood Flow Frequency,
962 Bulletin #17B of the Hydrology Subcommittee, Interagency Advisory Committee on
963 Water Data, US Geological Survey, Reston, VA, 1982.
- 964 Vale, M.: Securing the US Electrical Grid, Center for the Study of the Presidency and
965 Congress (CSPC), Washington DC, available at: [https://protectourpower.org/
966 resources/cspc-2014.pdf](https://protectourpower.org/resources/cspc-2014.pdf) (last access: 14 March 2017), 2014.
- 967 Wigmosta, M. S., Vail, L. W., and Lettenmaier, D. P.: A Distributed Hydrology-
968 Vegetation Model for Complex Terrain, *Water Resour. Res.*, 30(6), 1665–1679,
969 doi:10.1029/94WR00436, 1994.
- 970 Wigmosta, M. S., Nijssen, B., Storck, P., and Lettenmaier, D. P.: The Distributed
971 Hydrology Soil Vegetation Model, in *Mathematical Models of Small Watershed
972 Hydrology and Applications*, V. P. Singh, D. K. Frevert, eds., *Wat. Resour.
973 Publications*, Littleton, CO, 2002.
- 974 Wilbanks, T. J., Bhatt, V., Bilello, D., Bull, S., Ekmann, J., Horak, W., Huang, Y. J.,
975 Levine, M. D., Sale, M. J., Schmalzer, D., and Scott, M. J.: Effects of Climate
976 Change on Energy Production and Use in the United States, *US Climate Change
977 Science Program Synthesis and Assessment Product 4.5*, available at:
978 [https://digitalcommons.unl.edu/cgi/viewcontent.cgi?article=1005&context=usdoepub
979](https://digitalcommons.unl.edu/cgi/viewcontent.cgi?article=1005&context=usdoepub) (last access: 17 December 2019), 2008.
- 980 Wing, O. E. J., Bates, P. D., Sampson, C. C., Smith, A. M., Johnson, K. A., and Erickson,
981 T. A.: Validation of a 30 m Resolution Flood Hazard Model of the Conterminous



- 982 United States, *Water Resour. Res.*, 53, 7968–7986, doi:10.1002/2017WR020917,
983 2017.
- 984 Wing, O. E. J., Bates, P. D., Smith, A. M., Sampson, C. C., Johnson, K. A., Fargione, J.,
985 and Morefield, P.: Estimates of Present and Future Flood Risk in the Conterminous
986 United States, *Environ. Res. Lett.*, 13(3), 034023, doi:10.1088/1748-9326/aaac65,
987 2018.
- 988 Winkler, J., Duenas-Osorio, L., Stein, R., and Subramanian, D.: Performance Assessment
989 of Topologically Diverse Power Systems Subjected to Hurricane Events, *Reliability
990 Engineering and System Safety*, 95(4), 323–336, doi:10.1016/j.res.2009.11.002,
991 2010.
- 992 Winsemius, H. C., Aerts, J. C. J. H., van Beek, L. P. H., Bierkens, M. F. P., Bouwman,
993 A., Jongman, B., Kwadijk, J. C. J., Ligtoet, W., Lucas, P. L., van Vuuren, D. P., and
994 Ward, P. J.: Global Drivers of Future River Flood Risk, *Nat. Clim. Chang.*, 6, 381–
995 385, doi:10.1038/NCLIMATE2893, 2016.
- 996 Wobus, C., Gutmann, E., Jones, R., Rissing, M., Mizukami, N., Lorie, M., Mahoney, H.,
997 Wood, A. W., Mills, D., and Martinich, J.: Climate Change Impacts on Flood Risk
998 and Asset Damages within Mapped 100-year Floodplains of the Contiguous United
999 States, *Nat. Hazards Earth Syst. Sci.*, 17, 2199–2211, doi:10.5194/nhess-17-2199-
1000 2017, 2017.
- 1001 Zamuda, C., Antes, M., Gillespie, C. W., Mosby, A., and Zotter, B.: Climate Change and
1002 the US Energy Sector: Regional Vulnerabilities and Resilience Solutions, Office of
1003 Energy Policy and Systems Analysis, US Department of Energy, available at:



- 1004 [https://energy.gov/sites/prod/files/2015/10/f27/Regional_Climate_Vulnerabilities_and](https://energy.gov/sites/prod/files/2015/10/f27/Regional_Climate_Vulnerabilities_and_Resilience_Solutions_0.pdf)
1005 [Resilience_Solutions_0.pdf](https://energy.gov/sites/prod/files/2015/10/f27/Regional_Climate_Vulnerabilities_and_Resilience_Solutions_0.pdf) (last access: 17 December 2019), 2015.
- 1006 Zamuda, C. and Lippert, A.: Climate Change and the Electricity Sector: Guide for
1007 Assessing Vulnerabilities and Developing Resilience Solutions to Sea Level Rise,
1008 Office of Energy Policy and Systems Analysis, US Department of Energy, available
1009 at: [https://toolkit.climate.gov/sites/default/files/Climate%20Change%20](https://toolkit.climate.gov/sites/default/files/Climate%20Change%20and%20the%20Electricity%20Sector%20Guide%20for%20Assessing%20Vulnerabilities%20and%20Developing%20Resilience%20Solutions%20to%20Sea%20Level%20Rise%20July%202016.pdf)
1010 [and%20the%20Electricity%20Sector%20Guide%20for%20Assessing%20Vulnerabili](https://toolkit.climate.gov/sites/default/files/Climate%20Change%20and%20the%20Electricity%20Sector%20Guide%20for%20Assessing%20Vulnerabilities%20and%20Developing%20Resilience%20Solutions%20to%20Sea%20Level%20Rise%20July%202016.pdf)
1011 [ties%20and%20Developing%20Resilience%20Solutions%20to%20Sea%20Level%2](https://toolkit.climate.gov/sites/default/files/Climate%20Change%20and%20the%20Electricity%20Sector%20Guide%20for%20Assessing%20Vulnerabilities%20and%20Developing%20Resilience%20Solutions%20to%20Sea%20Level%20Rise%20July%202016.pdf)
1012 [0Rise%20July%202016.pdf](https://toolkit.climate.gov/sites/default/files/Climate%20Change%20and%20the%20Electricity%20Sector%20Guide%20for%20Assessing%20Vulnerabilities%20and%20Developing%20Resilience%20Solutions%20to%20Sea%20Level%20Rise%20July%202016.pdf) (last access: 18 December 2019), 2016.
- 1013 Zhao, G., Gao, H., Naz, B. S., Kao, S.-C., and Voisin, N.: Integrating a Reservoir
1014 Regulation Scheme into a Spatially Distributed Hydrological Model, *Adv. Water*
1015 *Resour.*, 98, 16–31, doi:10.1016/j.advwatres.2016.10.014, 2016.
- 1016 Zheng, X., Maidment, D. R., Tarboton, D. G., Liu, Y. Y., and Passalacqua, P.: GeoFlood:
1017 Large-scale Flood Inundation Mapping Based on High-Resolution Terrain Analysis,
1018 *Water Resour. Res.*, 54, 10,013–10,033, doi:10.1029/2018WR023457, 2018.